

1 **Temporary and net sinks of atmospheric CO₂ due to chemical**
2 **weathering in subtropical catchment with mixing carbonate and**
3 **silicate lithology**

4 Yingjie Cao^{a,c,d}, Yingxue Xuan^b, Changyuan Tang^{a,b,c*}, Shuai Guan^e, Yisheng Peng^{a,c}

5 ^aSchool of Environmental Science and Engineering, Sun Yat-Sen University, Guangzhou,
6 China

7 ^bSchool of Geography and Planning, Sun Yat-Sen University, Guangzhou, China

8 ^cGuangdong Provincial Key Laboratory of Environmental Pollution Control and Remediation
9 Technology, Sun Yat-Sen University, Guangzhou, China

10 ^dSouthern Marine Science and Engineering Guangdong Laboratory, Zhuhai, China

11 ^eGuangdong Research Institute of Water Resource and Hydropower, Guangzhou, China

12
13 **Abstract:** The study provided the major ion chemistry, chemical weathering rates and temporary
14 and net CO₂ sinks in the Beijiang River, which was characterized as hyperactive region with high
15 chemical weathering rates, carbonate and silicate mixing lithology and abundant sulfuric acid
16 chemical weathering agent of acid deposition and acid mining drainage (AMD) origins. The total
17 chemical weathering rate of 85.46 t·km⁻²·a⁻¹ was comparable to other rivers in the hyperactive
18 zones between the latitude 0-30°. Carbonate weathering rate of 61.15 t·km⁻²·a⁻¹ contributed to
19 about 70% of the total. The lithology, runoff and geomorphology had significant influence on the
20 chemical weathering rate. The proportion of carbonate outcrops had significant positive
21 correlation with the chemical weathering rate. Due to the interaction between dilution and
22 compensation effect, significant positive linear relationship was detected between runoff and total,

23 carbonate and silicate weathering rates. The geomorphology factors such as catchment area,
24 average slope and hypsometric integral value (HI) had non-linear correlation with chemical
25 weathering rate and showed significant scale effect, which revealed the complexity in chemical
26 weathering processes. DIC-apportionment showed that CCW (Carbonate weathering by CO₂) was
27 the dominant origin of DIC (35%-87%). SCW (Carbonate weathering by H₂SO₄) (3%-15%) and
28 CSW (Silicate weathering by CO₂) (7%-59%) were non-negligible processes. The temporary CO₂
29 sink was 823.41 10³ mol km⁻² a⁻¹. Compared with the “temporary” sink, the net sink of CO₂ for the
30 Beijiang River was approximately 23.18×10³ mol km⁻² a⁻¹ of CO₂ and was about 2.82% of the
31 “temporary” CO₂ sink. Human activities (sulfur acid deposition and AMD) dramatically decreased
32 the CO₂ net sink and even make chemical weathering a CO₂ source to the atmosphere.

33 **Keywords:** Chemical weathering, DIC-apportionment, CO₂ temporary sink, CO₂ net sink

34 **1 Introduction**

35 About half of the global CO₂ sequestration due to chemical weathering occurs in warm and
36 high runoff regions (Ludwig et al., 1998), so called the hyperactive regions and hotspots
37 (Meybeck et al., 2006). **Chemical weathering driven by weak carbonic acid (H₂CO₃) that
38 originates from atmosphere CO₂ or soil respiration under natural conditions is a fundamental
39 geochemical process regulating the atmosphere-land-ocean carbon fluxes and earth’s climate (Guo
40 et al., 2015). Carbonate and silicate weathering define the two typical categories of chemical
41 weathering. From the view of the global carbon cycle, the CO₂ consumption due to carbonate
42 weathering is recognized the “temporary” sink because the flux of CO₂ consumed by carbonate
43 dissolution on the continents is balanced by the flux of CO₂ released into the atmosphere from the
44 oceans by carbonate precipitation on the geological time scale (Cao et al., 2015; Garrels, 1983).**

45 While the consumption of CO₂ during the chemical weathering of silicate rocks has been regard as
46 the net sink of CO₂ and regulates the global carbon cycle (Hartmann et al., 2009; Hartmann et al.,
47 2014b; Kempe and Degens, 1985; Lenton and Britton, 2006). Thus in carbonate-silicate mixing
48 catchment, it is essential to distinguish proportions of the two most important lithological groups,
49 i.e., carbonates and silicates, and evaluate the net CO₂ sink due to chemical weathering of silicate
50 (Hartmann et al., 2009).

51 In addition to the chemical weathering induced by H₂CO₃, sulfuric acid (H₂SO₄) of
52 anthropogenic origins produced by sulfide oxidation such as acid deposition caused by fossil fuel
53 burning and acid mining discharge (AMD) also becomes an important chemical weathering agent
54 in the catchment scale. Many studies have shown the importance of sulfide oxidation and
55 subsequent dissolution of other minerals by the resulting sulfuric acid at catchment scale (Hercod
56 et al., 1998; Spence and Telmer, 2005). Depending on the fate of sulfate in the oceans, sulfide
57 oxidation coupled with carbonate dissolution could facilitate a release of CO₂ to the atmosphere
58 (Spence and Telmer, 2005), the carbonate weathering by H₂SO₄ plays a very important role in
59 quantifying and validating the ultimate CO₂ consumption rate. Thus, under the influence of human
60 activities, the combination of silicate weathering by H₂CO₃ and carbonate weathering by H₂SO₄
61 controlled the net sink of atmospheric CO₂.

62 Numerous studies on chemical weathering of larger rivers have been carried out to examine
63 hydrochemical characteristics, chemical erosion and CO₂ consumption rates, and long-term
64 climatic evolution of the Earth, such as the Changjiang River (Chen et al., 2002a; Ran et al., 2010),
65 the Huanghe River (Zhang et al., 1995), the Pearl River (Gao et al., 2009; Xu and Liu, 2010;
66 Zhang et al., 2007a), the Huai River (Zhang et al., 2011), the rivers of the Qinghai-Tibet Plateau

67 (Jiang et al., 2018; Li et al., 2011; Wu et al., 2008), the Mekong River (Li et al., 2014), the rivers
68 of the Alpine region (Donnini et al., 2016), the Sorocabá River (Fernandes et al., 2016), the rivers
69 of Baltic Sea catchment (Sun et al., 2017), the Amazon River (Gibbs, 1972; Mortatti and Probst,
70 2003; Stallard and Edmond, 1981; Stallard and Edmond, 1983; Stallard and Edmond, 1987), the
71 Lena River (Huh and Edmond, 1999) and the Orinoco River (Mora et al., 2010). For simplicity of
72 calculation procedure, most of the researches have **ignored** the sulfuric acid induced chemical
73 weathering and resulted in an overestimation of CO₂ sink. To overcome this shortcoming of
74 traditional mass-balance method, we applied a DIC source apportionment procedure to
75 discriminate the contribution of sulfuric acid induced chemical weathering to validate the
76 temporary and net sink of CO₂ in a typical hyperactive region with carbonate-silicate mixing
77 lithology to give a further understanding of basin scale chemical weathering estimation.

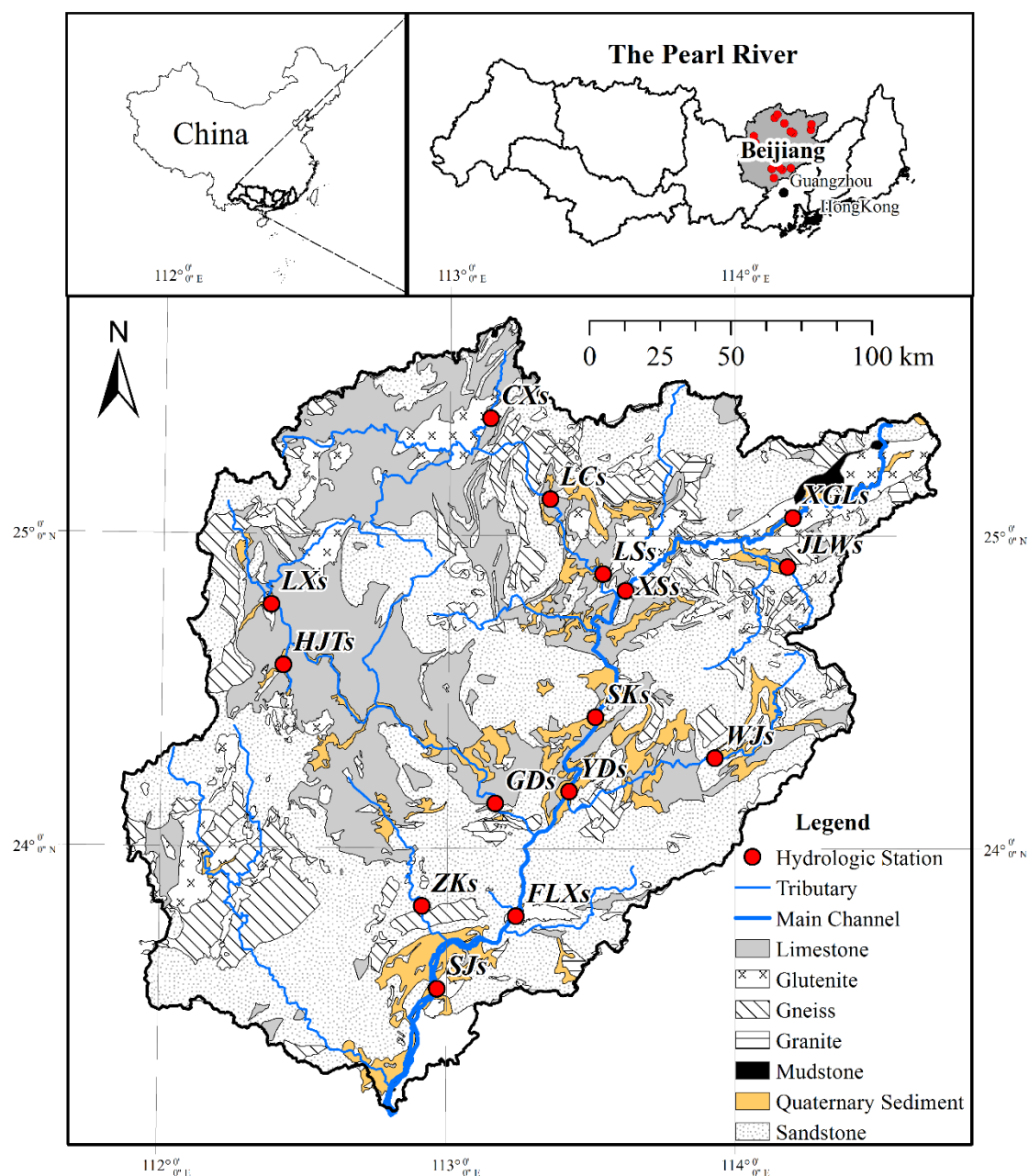
78 The Pearl River located in the subtropical area in South China includes three principal rivers:
79 the Xijiang, Beijiang, and Dongjiang Rivers. The warm and wet climatic conditions make the
80 Pearl River a hyperactive region in China. The three river basins have distinct geological
81 conditions. The Xijiang River is characterized as the carbonate-dominated area and the Dongjiang
82 River has silicate as the main rock type. While the Beijiang River, which is the second largest
83 tributary of the Pearl River, is characterized as a typical carbonate-silicate mixing basin. In
84 addition, as the serve acid deposition (Larssen et al., 2006) and active mining area (Li et al., 2019),
85 chemical weathering induced by sulfuric acid make the temporary and net sink of atmospheric
86 CO₂ to be reevaluated. So that, in this study, the Beijiang River in Southeast China with a typical
87 subtropical monsoon climate and carbonate-silicate mixing geologic settings was selected as the
88 study area. Three main objectives were summarized as follows: (1) revealed spatial-temporal

89 variations of major element chemistry of the river water, (2) calculated the chemical weathering
90 rate and unraveled the controlling factors on chemical weathering processes, and (3) determined
91 the temporary sink of CO₂ and evaluated the influence of sulfide oxidation on net sink of CO₂ by
92 DIC apportionment procedure.

93 **2 Study area**

94 The Beijiang River Basin, which is the second largest tributary of the Pearl River Basin, is
95 located in the southeast of China (Fig. 1). It covers an area of 52 068 km² and has a total length of
96 573 km. The river basin is located in subtropical monsoon climate zone, with the mean annual
97 temperature across the drainage basin ranging from 14°C to 22°C, the mean annual precipitation
98 ranging from 1390 mm to 2475 mm. The average annual runoff is 51 billion m³, with 70%-80% of
99 the flux occurring from April to September. This can be attributed to the fact that more than 70% of
100 the annual precipitation (about 1800 mm year⁻¹) is concentrated in the wet season (April to
101 September).

102 Lithology in the river basin is composed of limestone, sandstone, gneiss and glutenite. In the
103 upper basin, carbonate rock (mainly of limestone) outcrops in the west and center, while sandstone
104 of Devonian era and mudstone of Paleogene era outcrop in the east of upper stream. In the middle of
105 basin, limestone and sandstone cover most of the area, and Cretaceous volcanic rocks are found in
106 the tributary (Lianjiang River), mainly granite. In the lower basin, Achaen metamorphic rocks
107 outcrop in the west, and are composed of gneiss and schist, sandstone covers rest of area of the
108 lower basin. Quaternary sediments scatter along the main stream of the river. The carbonate and
109 silicate rock outcrops in the Beijiang River Basin was 10737 km² (28%) and 24687 km² (65%),
110 respectively.



111
112 **Fig. 1** Geology map and sampling point in the Beijiang River basin by ArcGis

113 **3 Materials and methods**

114 **3.1 Sampling procedure and laboratory analysis**

115 Water samples were collected monthly at 15 hydrologic stations from January to December in
116 2015 (Fig. 1). The river waters were sampled by a portable organic class water sampler along the
117 middle thread of channel in the first day of each month. In addition, to discriminate the contribution
118 of rain inputs, the daily rainwater was also sampled in five stations (SJs, FLXs, YDs, XSs and XGLs)

119 along the main stream. The rainwater collector is consisted of a funnel with diameter of 20 cm and a
120 5 L plastic bottle. A rubber ball is setup in the funnel to prevent evaporation. All the river and rain
121 water were filtered through 0.45 μm glass fiber filter and stored in 100 ml tubes and stored below
122 4°C until analysis.

123 Electric conductivity (EC), pH and temperature (T) were measured by a multi-parameter water
124 quality meter (HACH-HQ40Q), and alkalinity (HCO_3^-) was measured in filtered water samples by
125 titration in situ. The dissolved SiO_2 was measured by molybdenum yellow method and was
126 analyzed by ultraviolet spectrophotometer (Shimadzu UV-2600). The cations (Na^+ , K^+ , Ca^{2+} ,
127 Mg^{2+}) and anions (Cl^- , SO_4^{2-}) were analyzed by ion chromatography (ThermoFisher ICS-900)
128 with limit of detection (L.O.D) of 0.01 mg/L. Reference, blank and replicate samples were
129 employed to check the accuracy of all the analysis and the relative standard deviations of all the
130 analysis were within $\pm 5\%$. The electrical balance (E.B.) defined by the equation of E.B. =
131 $\frac{\text{meq}(\text{sum of cations}) - \text{meq}(\text{sum of anions})}{\text{meq}(\text{sum of cations and anions})} \times 100$ of the water samples was less than 5%.

132 3.2 Calculation procedure

133 3.2.1 Chemical weathering rates

134 The mass balance equation for element X in the dissolved load can be expressed as (Galy and
135 France-Lanord, 1999):

$$136 \quad [X]_{\text{riv}} = [X]_{\text{pre}} + [X]_{\text{eva}} + [X]_{\text{sil}} + [X]_{\text{car}} + [X]_{\text{anth}} \quad (1)$$

137 Where $[X]$ denotes the elements of Ca^{2+} , Mg^{2+} , Na^+ , K^+ , Cl^- , SO_4^{2-} , HCO_3^- in $\text{mmol}\cdot\text{L}^{-1}$. The
138 subscripts riv, pre, eva, sil, car and anth denote the river, precipitation source, evaporite source,
139 silicate source, carbonate source and anthropogenic source. The hydrochemical compositions of
140 rain water were summarized in Table S1 in the supplementary materials.

141 In the study area, the anthropogenic source of major ions except for SO_4^{2-} was ignored due to
 142 the following two reasons. (1) Two main characteristics of much polluted rivers are that TDS is
 143 greater than 500 mg/L and the Cl^-/Na^+ molar ratio is greater than that of sea salts (about 1.16)
 144 (Cao et al., 2016a; Gaillardet et al., 1999b). The TDS in the study area ranged from 73.79 to
 145 230.16 $\text{mg}\cdot\text{L}^{-1}$ and the low TDS implied that the anthropogenic origins of major ions could be
 146 ignored in the study. However, the Beijiing River is characterized as a typical region suffered
 147 from severe acid deposition (Larsen et al., 2006) and active mining area (Li et al., 2019). The acid
 148 deposition and acid mining discharge contribute to the highest concentration of SO_4^{2-} . (2) Natural
 149 origin of SO_4^{2-} is the dissolution of evaporite, such as gypsum, while no evaporite was found in
 150 the study area. If SO_4^{2-} comes from the gypsum dissolution, the ratios of Ca^{2+} and SO_4^{2-} should be
 151 close to 1:1. The stoichiometric analysis (Fig.11) showed that the ratio of Ca^{2+} and SO_4^{2-} deviated
 152 from 1:1 and also proved this point.

153 So that, on the basis of the theory of rock chemical weathering and ignoring the
 154 anthropogenic origins of major ions (except for SO_4^{2-}), the major elements of river water can be
 155 simplified as followed:

$$156 \quad [\text{Cl}^-]_{\text{riv}} = [\text{Cl}^-]_{\text{pre}} + [\text{Cl}^-]_{\text{eva}} \quad (2)$$

$$157 \quad [\text{K}^+]_{\text{riv}} = [\text{K}^+]_{\text{pre}} + [\text{K}^+]_{\text{sil}} \quad (3)$$

$$158 \quad [\text{Na}^+]_{\text{riv}} = [\text{Na}^+]_{\text{pre}} + [\text{Na}^+]_{\text{eva}} + [\text{Na}^+]_{\text{sil}} \quad (4)$$

$$159 \quad [\text{Ca}^{2+}]_{\text{riv}} = [\text{Ca}^{2+}]_{\text{pre}} + [\text{Ca}^{2+}]_{\text{sil}} + [\text{Ca}^{2+}]_{\text{car}} \quad (5)$$

$$160 \quad [\text{Mg}^{2+}]_{\text{riv}} = [\text{Mg}^{2+}]_{\text{pre}} + [\text{Mg}^{2+}]_{\text{sil}} + [\text{Mg}^{2+}]_{\text{car}} \quad (6)$$

$$161 \quad [\text{HCO}_3^-]_{\text{sil}} = [\text{K}^+]_{\text{sil}} + [\text{Na}^+]_{\text{sil}} + 2[\text{Mg}^{2+}]_{\text{sil}} + 2[\text{Ca}^{2+}]_{\text{sil}} \quad (7)$$

$$162 \quad [\text{HCO}_3^-]_{\text{car}} = [\text{HCO}_3^-]_{\text{riv}} - [\text{HCO}_3^-]_{\text{sil}} \quad (8)$$

163 $[\text{SO}_4^{2-}]_{\text{riv}} = [\text{SO}_4^{2-}]_{\text{pre}} + [\text{SO}_4^{2-}]_{\text{anth}}$ (9)

164 Firstly, the measured ion concentrations of the rain water are rectified by evaporation
 165 coefficient $\alpha=0.63=P/R$ (with P the precipitation and R the runoff) and calculated the contributions
 166 of atmospheric precipitation. Secondly, the molar ratios of $\text{Ca}^{2+}/\text{Na}^+$ (0.4) and $\text{Mg}^{2+}/\text{Na}^+$ (0.2) for
 167 silicate end-member (Zhang et al., 2007b) are used to calculate the contribution of Ca^{2+} and Mg^{2+}
 168 from silicate weathering, and then, residual Ca^{2+} and Mg^{2+} were attributed to carbonate weathering.
 169 For monthly data, the contributions of different sources can be calculated as followed:

170 $R_{\text{car}} = ([\text{Ca}^{2+}]_{\text{car}} + [\text{Mg}^{2+}]_{\text{car}}) / S \times 100\%$ (10)

171 $R_{\text{sil}} = ([\text{K}^+]_{\text{sil}} + [\text{Na}^+]_{\text{sil}} + [\text{Ca}^{2+}]_{\text{sil}} + [\text{Mg}^{2+}]_{\text{sil}}) / S \times 100\%$ (11)

172 $R_{\text{eva}} = [\text{Na}^+]_{\text{eva}} / S \times 100\%$ (12)

173 $R_{\text{pre}} = ([\text{K}^+]_{\text{pre}} + [\text{Na}^+]_{\text{pre}} + [\text{Ca}^{2+}]_{\text{pre}} + [\text{Mg}^{2+}]_{\text{pre}}) / S \times 100\%$ (13)

174 $S = [\text{Ca}^{2+}]_{\text{car}} + [\text{Mg}^{2+}]_{\text{car}} + [\text{Ca}^{2+}]_{\text{sil}} + [\text{Mg}^{2+}]_{\text{sil}} + [\text{Na}^+]_{\text{sil}} + [\text{K}^+]_{\text{sil}} + [\text{Na}^+]_{\text{eva}} +$
 175 $[\text{Ca}^{2+}]_{\text{pre}} + [\text{Mg}^{2+}]_{\text{pre}} + [\text{Na}^+]_{\text{pre}} + [\text{K}^+]_{\text{pre}}$ (14)

176 Where R denotes the proportions of dissolved cations from different sources. S denotes the total
 177 concentrations of cations for river water in $\text{mmol}\cdot\text{L}^{-1}$.

178 The total, carbonate and silicate chemical weathering rates (TWR, CWR and SWR) of a year
 179 can be estimated as followed:

180 $\text{CWR} = \sum_{i=1}^{n=12} [(24 \times [\text{Mg}^{2+}]_{\text{car}} + 40 \times [\text{Ca}^{2+}]_{\text{car}} + 61 \times [\text{HCO}_3^-]_{\text{car}} \times 0.5)_i \times Q_i / (10^6 \text{A})]$ (15)

181 $\text{SWR} = \sum_{i=1}^{n=12} [(39 \times [\text{K}^+]_{\text{sil}} + 23 \times [\text{Na}^+]_{\text{sil}} + 24 \times [\text{Mg}^{2+}]_{\text{sil}} + 40 \times [\text{Ca}^{2+}]_{\text{sil}} + 96 \times [\text{SiO}_2]_{\text{sil}})_i \times$
 182 $Q_i / (10^6 \text{A})]$ (16)

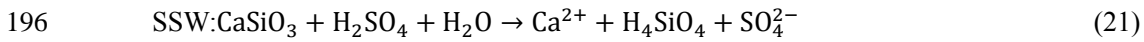
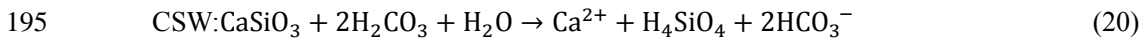
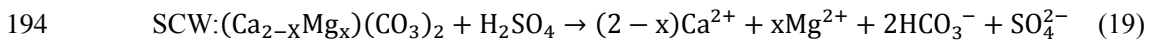
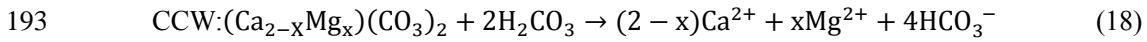
183 $\text{TWR} = \text{CWR} + \text{SWR}$ (17)

184 Where TWR, CWR and SWR have the unit of $\text{t km}^{-2} \text{a}^{-1}$, Q_i denotes discharge in $\text{m}^3 \cdot \text{month}^{-1}$, and

185 A denotes the catchment area in km².

186 3.2.2 DIC apportionments

187 The riverine DIC originates from several sources including carbonate minerals, respired soil
188 CO₂ and atmospheric CO₂, and it could be affected by processes occurring along the water
189 pathways (Khadka et al., 2014; Li et al., 2008). Four dominant weathering processes, including (1)
190 carbonate weathering by carbonic acid (CCW), (2) carbonate weathering by sulfuric acid (SCW),
191 (3) silicate weathering by carbonic acid (CSW), (4) and silicate weathering by sulfuric acid (SSW),
192 can be described by the following reaction equations:



197 Where CaSiO₃ represents an arbitrary silicate.

198 According to the study of Galy and France-Lanord (1999) and Spence and Telmer (2005),
199 carbonate and silicate weathering by carbonic acid in the same ratio as carbonate and silicate
200 weathering by sulfuric acid, for monthly data the mass balance equations are followed:

$$201 \quad [\text{SO}_4^{2-}]_{\text{riv}} - [\text{SO}_4^{2-}]_{\text{pre}} = [\text{SO}_4^{2-}]_{\text{scw}} + [\text{SO}_4^{2-}]_{\text{ssw}} \quad (22)$$

$$202 \quad [\text{SO}_4^{2-}]_{\text{riv}} - [\text{SO}_4^{2-}]_{\text{pre}} = \alpha_{\text{scw}} \times [\text{HCO}_3^-]_{\text{riv}} \times 0.5 + \frac{\alpha_{\text{csw}} \times \alpha_{\text{scw}}}{\alpha_{\text{ccw}}} \times [\text{HCO}_3^-]_{\text{riv}} \quad (23)$$

203 Where the subscripts CCW, SCW, CSW and SSW denotes the four end-members defined by
204 carbonate weathering by carbonic acid, carbonate weathering by sulfuric acid, silicate weathering
205 by carbonic acid and silicate weathering by sulfuric acid, respectively. The parameter α denotes
206 the proportion of DIC derived from each end-member processes.

207 According to the above description, the ion balance equations are followed:

$$208 \quad [\text{Ca}^{2+}]_{\text{car}} + [\text{Mg}^{2+}]_{\text{car}} = \alpha_{\text{CCW}} \times [\text{HCO}_3^-]_{\text{riv}} \times 0.5 + \alpha_{\text{SCW}} \times [\text{HCO}_3^-]_{\text{riv}} \quad (23)$$

$$209 \quad [\text{SO}_4^{2-}]_{\text{SCW}} + [\text{SO}_4^{2-}]_{\text{SSW}} = \alpha_{\text{SCW}} \times [\text{HCO}_3^-]_{\text{riv}} \times 0.5 + \frac{\alpha_{\text{CSW}} \times \alpha_{\text{SCW}}}{\alpha_{\text{CCW}}} \times [\text{HCO}_3^-]_{\text{riv}} \quad (24)$$

$$210 \quad \alpha_{\text{CCW}} + \alpha_{\text{SCW}} + \alpha_{\text{CSW}} = 1 \quad (25)$$

211 Combing the above equations, the proportions of HCO_3^- derived from three end-members
212 (CCW, SCW and CSW) can be calculated, and the DIC (equivalent to HCO_3^-) fluxes by different
213 chemical weathering processes are calculated by following equations.

$$214 \quad \text{DIC}_{\text{CCW}} = \alpha_{\text{CCW}} \times [\text{HCO}_3^-]_{\text{riv}} \quad (26)$$

$$215 \quad \text{DIC}_{\text{SCW}} = \alpha_{\text{SCW}} \times [\text{HCO}_3^-]_{\text{riv}} \quad (27)$$

$$216 \quad \text{DIC}_{\text{CSW}} = \alpha_{\text{CSW}} \times [\text{HCO}_3^-]_{\text{riv}} \quad (28)$$

217 **3.2.3 CO₂ consumption rate and CO₂ net sink**

218 According to the equations (17)~(20), only the processes of CCW and CSW can consume
219 the CO₂ from atmosphere or soil and only half of the HCO_3^- in the water due to carbonate
220 weathering by carbonic acid come from atmospheric CO₂. Thus, the CO₂ consumption rates (CCR)
221 for CCW and CSW can be calculated as followed (Zeng et al., 2016):

$$222 \quad \text{CCR}_{\text{CCW}} = \sum_{i=1}^{n=12} \{ [0.5 \times (Q/A) \times [\text{HCO}_3^-]_{\text{CCW}}] / 1000 \}_i \quad (29)$$

$$223 \quad \text{CCR}_{\text{CSW}} = \sum_{i=1}^{n=12} \{ [(Q/A) \times [\text{HCO}_3^-]_{\text{CSW}}] / 1000 \}_i \quad (30)$$

224 Where Q is discharge in $\text{m}^3 \cdot \text{a}^{-1}$, $[\text{HCO}_3^-]$ is concentration of HCO_3^- in $\text{mmol} \cdot \text{L}^{-1}$, A is catchment
225 area in km^2 , so that the CCR has the unit of $10^3 \text{ mol km}^{-2} \cdot \text{a}^{-1}$.

226 According to the classical view of the global carbon cycling (Bernier and Kothavala, 2001),
227 the CCW is not a mechanism that can participate to the amount of CO₂ in the atmosphere because
228 all of the atmospheric fixed through CCW is returned to the atmosphere during carbonate

229 precipitation in the ocean. However, when sulfuric acid is involved as a proton donor in carbonate
 230 weathering, half of the dissolved carbon re-release to the atmospheric during carbonate
 231 precipitation. Thus, SCW leads to a net release of CO₂ in ocean-atmosphere system over timescale
 232 typical of residence time of HCO₃⁻ in the ocean (10⁵ years). Meanwhile, in case of CSW, followed
 233 by carbonate deposition, one of the two moles of CO₂ involved is transferred from the atmosphere
 234 to the lithosphere in the form of carbonate rocks, while the other one returns to the atmosphere,
 235 resulting a net sink of CO₂. Therefore, the net CO₂ consumption rate (CCR_{Net}) due to chemical
 236 weathering can be concluded as followed:

$$237 \quad CCR_{Net} = \sum_{i=1}^{n=12} \{[(0.5 \times [HCO_3^-]_{CSW} - 0.5 \times [HCO_3^-]_{SCW}) \times (Q/A)]/1000\}_i \quad (31)$$

238 **3.3 Spatial and statistical analysis**

239 The hypsometric integral value (HI) (PIKE and WILSON, 1971) was employed in this study
 240 to evaluate the influence of terrain on the chemical weathering. HI is an important index to reveal
 241 the relationship between morphology and development of landforms and can be used to establish
 242 the quantitative relationship between the stage of geomorphological development and the material
 243 migration in the basin (PIKE and WILSON, 1971; Singh et al., 2008; STRAHLER, 1952). The HI
 244 value of each watershed is calculated by the elevation-relief ratio method and can be obtained by
 245 the following equation (PIKE and WILSON, 1971):

$$246 \quad HI = \frac{\text{Mean.elevation} - \text{Min.elevation}}{\text{Max.elevation} - \text{Min.elevation}} \quad (32)$$

247 Where HI is the hypsometric integral; Mean.elevation is the mean elevation of the watershed;
 248 Min.elevation is the minimum elevation within the watershed; Max.elevation is the maximum
 249 elevation within the watershed. According to the hypsometric integral value (HI), the
 250 geomorphological development can be divided into three stages: inequilibrium or young stage (HI >

251 0.6), equilibrium or mature stage ($0.35 < HI \leq 0.6$), and monadnock or old age ($HI \leq 0.35$),
252 which can reflect the erodible degree and erosion trend of the geomorphology (Xiong et al., 2014).

253 The watershed of the study area was divided by using hydrological analysis module of
254 ArcGIS. The average slope and HI was conducted by spatial analysis module of ArcGIS. **The area
255 of silicate/carbonate outcrops was calculated by hydrological module of ArcGIS based on geology
256 map from provided by China Geological Survey. The data of river water discharge was provided
257 by the local hydrology bureau.**

258 All statistical tests were conducted using SPSS version 22.0. One-way analysis of variance
259 (ANOVA) was performed to check the differences of monthly major ion concentrations and
260 dissolved inorganic carbonate isotopes with significance at $p < 0.05$. Principal component analysis
261 (PCA) was employed to unravel the underlying data set through the reduced new variables,
262 analyzed the significant factors affecting the characteristics of water chemistry.

263 **4 Results**

264 **4.1 Chemical compositions**

265 The major physical-chemical parameters of river water samples were presented in Table 1. **In
266 Table 1, the chemical parameters of river water were the flow-weighted average over 12 months.
267 For every sampling station, the flow-weighted average of ion concentration can be expressed
268 followed the equation $[X]_{average} = \frac{\sum_{i=1}^{n=12} [X]_i \times Q_i}{\sum_{i=1}^{n=12} Q_i}$, where $[X]$ denotes the elements of Ca^{2+} , Mg^{2+} ,
269 Na^+ , K^+ , Cl^- , SO_4^{2-} , HCO_3^- in $mmol \cdot L^{-1}$. Q denotes average monthly discharge in $m^3 \cdot s^{-1}$. The
270 subscripts i denotes 12 months from January to December. For all the monthly samples, the pH
271 values ranged from 7.5 to 8.5 with an average of 8.05. Average EC was $213 \mu s \cdot cm^{-1}$, ranging from
272 81 to $330 \mu s \cdot cm^{-1}$. The TDS of river water samples varied from 73.8 to $230.2 mg \cdot L^{-1}$, with an**

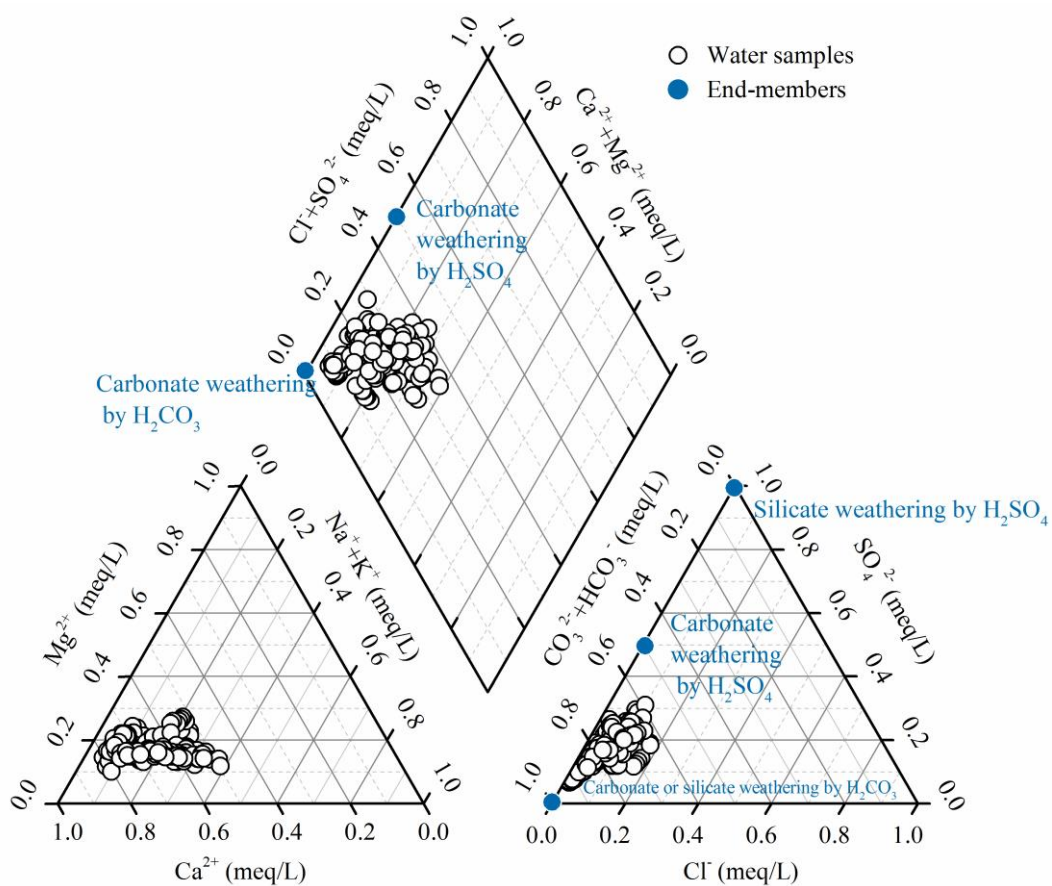
273 average of $157.3 \text{ mg}\cdot\text{L}^{-1}$, which was comparable with the global average of $100 \text{ mg}\cdot\text{L}^{-1}$ (Gaillardet
274 et al., 1999a). Compared with the major rivers in China, the average TDS was significantly lower
275 than the Changjiang (Chen et al., 2002b), the Huanghe (He Jiangyi, 2017) the Zhujiang (Zhang et
276 al., 2007b), the Huaihe (Zhang et al., 2011) and the Liaohe (Ding et al., 2017). However, the
277 average TDS was higher than the rivers draining silicate-rock-dominated areas, e.g., Dojiang
278 River ($59.9 \text{ mg}\cdot\text{L}^{-1}$) in Southern China (Xie Chenji, 2013), North Han River ($75.5 \text{ mg}\cdot\text{L}^{-1}$) in
279 South Korea, (Ryu et al., 2008), the Amazon ($41 \text{ mg}\cdot\text{L}^{-1}$) and the Orinoco ($82 \text{ mg}\cdot\text{L}^{-1}$) draining the
280 Andes (Dosseto et al., 2006; Edmond et al., 1996).

281

282 **Table 1 The major physical-chemical parameters of river water samples at 15 hydrological station in the Beijiang River (mean \pm SD). The total dissolved solid**
 283 **(TDS, mg·L⁻¹) expressed as the sum of major inorganic species concentration (Na⁺+K⁺+Ca²⁺+Mg²⁺+HCO₃⁻+Cl⁻+SO₄²⁻+NO₃⁻+SiO₂)**

Hydrological stations	pH	EC (μs/cm)	TDS (mg/L)	Na ⁺ (μmol/L)	K ⁺ (μmol/L)	Ca ²⁺ (μmol/L)	Mg ²⁺ (μmol/L)	HCO ₃ ⁻ (μmol/L)	Cl ⁻ (μmol/L)	SO ₄ ²⁻ (μmol/L)	SiO ₂ (μmol/L)	HI
JLWs	7.9±0.15	95±39.98	81.1±25.6	111.4	51.9	223.5	103.9	701.9	28.3	44.5	225.2	0.3444
CXs	8.2±0.15	219±50.32	163.7±20.9	118.1	40.1	793.3	187.1	1593.6	60.5	199.4	106.3	0.2865
HJTs	8.1±0.19	203±34.39	151.8±21.9	100.2	29.9	686.7	203.9	1708.7	29.5	72.2	156.6	0.2991
ZKs	8.1±0.13	218±44.84	161.3±21.1	426.4	66.2	560.3	134.1	1276.9	134.7	161.4	151.9	0.2233
XGLs	7.8±0.15	168±15.83	117.9±8.9	315.4	112.4	422.4	101.0	992.2	213.9	112.6	178.9	0.1821
WJs	8.1±0.1	260±26.91	172.9±16.7	197.8	59.0	767.3	122.6	1467.1	99.1	162.8	183.4	0.2462
LXs	8.1±0.16	236±32.99	171.8±19.6	122.1	38.1	813.5	176.0	1829.4	51.5	89.2	145.7	0.2149
LCs	8.2±0.09	253±25.91	196.1±20.0	287.4	46.8	862.6	234.4	1845.7	115.7	232.4	130.7	0.2731
LSs	8.3±0.06	220±45.62	184.2±18.3	258.9	58.2	793.5	202.9	1740.6	109.0	191.9	121.4	0.2503
XSs	7.9±0.14	156±29.8	123.9±17.6	305.0	86.1	366.8	110.9	966.6	103.8	166.5	218.7	0.2365
GDs	8.1±0.05	232±10.67	169.4±8.3	112.6	40.5	781.6	172.1	1798.5	44.0	90.3	141.2	0.2415
SKs	8.1±0.19	238±21.6	161.1±17.4	345.3	73.6	641.0	162.5	1304.1	174.4	223.5	160.1	0.2061
Yds	7.8±0.2	241±54.39	165.9±34.0	296.4	59.3	674.8	160.9	1515.0	118.7	175.9	144.4	0.2055
FLXs	8±0.21	232±36.99	161.4±22.8	187.6	95.1	577.0	135.0	1262.4	111.9	159.6	169.5	0.2065
SJs	8.1±0.1	230±26.94	176.4±18.9	355.0	83.4	663.5	156.2	1367.7	182.4	190.5	180.5	0.2057

284 Major ion compositions were shown in the Piper plot (Fig. 2). Ca^{2+} was the dominant cation
 285 with concentration ranging from 199 to 1107 $\mu\text{mol}\cdot\text{L}^{-1}$, accounting for approximately 49% to 81%,
 286 with an average of 66% (in μEq) of the total cation composition in the river water samples. HCO_3^-
 287 was the dominant anion, with concentration ranging from 640 to 2289 $\mu\text{mol}\cdot\text{L}^{-1}$. On average, it
 288 comprised 77% (59%~92%) of total anions, followed by SO_4^{2-} (16%) and Cl^- (6%). The major
 289 ionic composition indicated that the water chemistry of the Beijiang River Basin was controlled by
 290 both carbonate and silicate weathering.



291

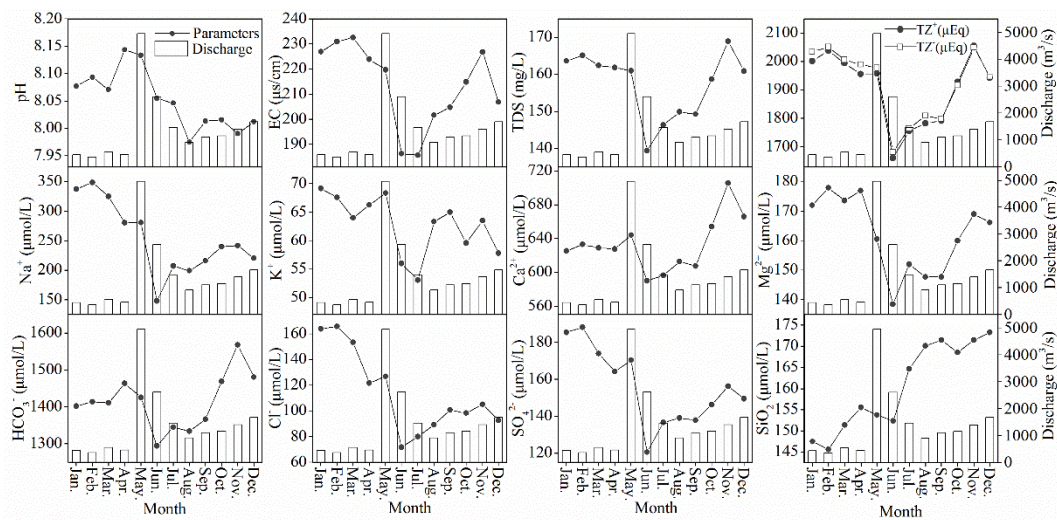
292 **Fig. 2 Piper plot of river water samples in the Beijiang River**

293 The PCA was used to extract the factors controlling the chemical compositions. The varimax
 294 rotation was used to reduce the number of variables to two principal components (PCs), which
 295 together explain 76.88% of the total variance in the data. The first PC (PC1) explained

296 approximately 50.02% of the total variations, and was considered to represent “carbonate
 297 weathering factor” because of the high loadings of EC, TDS, Ca²⁺, Mg²⁺ and HCO₃⁻
 298 concentrations. The second PC (PC2) explained 26.85% of the total variance and presented high
 299 loadings for Na⁺ and K⁺ concentrations. Thus, the PC2 represented a “silicate weathering factor”.
 300 These two PCs were considered to be two important sources of major ions in the Beijiang River
 301 Basin.

302 4.2 Seasonal and spatial variations

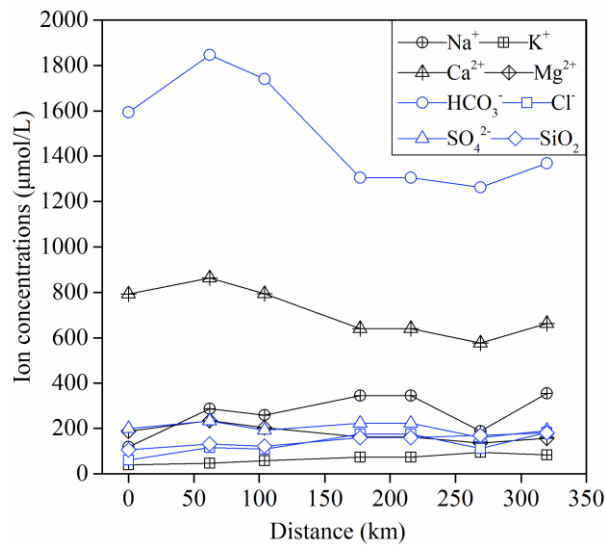
303 There were significant seasonal variations in the major ion concentrations (Fig. 3). Two basic
 304 patterns of temporal variations could be observed. The first one was related to the carbonate
 305 weathering derived ions such as Ca²⁺ and HCO₃⁻, which showed high values in November and low
 306 values in June. The second one was for the silicate weathering derived ions such as Na⁺ and K⁺,
 307 which showed high values in February and low values in June. The minimums occurred in Jun for
 308 all the ions showed a significant dilution effect during the high-flow periods.



309
 310 **Fig. 3 Monthly variations of environmental parameters and major ion concentrations in the**
 311 **Beijiang River Basin (SJs station). The columns denoted the monthly discharge**

312 It was clear that the Ca²⁺ and HCO₃⁻ concentrations had a decreasing trend from upstream to

313 **downstream** (Fig. 4), this characteristic agrees with the trends observed in the Changjiang River
 314 and the Huai River, where the major elements or TDS concentrations of the main channel showed
 315 a general decreasing trend, and the tributaries display the dilution effect to the main channel. For
 316 other silicate weathering derived ions such as Na^+ , there was a slight increasing trend implying the
 317 chemical inputs from the tributaries. These trends were in accordance with the lithology in the
 318 study area. The carbonate is dominated in the upper stream basin, when river drainages this area,
 319 carbonate weathering contributes to the elevation of Ca^{2+} and HCO_3^- . As the river entered into the
 320 downstream dominated with silicate, the relative low ion concentrations due to silicate weathering
 321 contributed to diluting the Ca^{2+} and introducing extra Na^+ to the main channel.



322
 323 **Fig. 4 Spatial variations of major ion and SiO₂ concentrations in the Beijiing River Basin (From**
 324 **upstream station CXs to the downstream station SJs)**

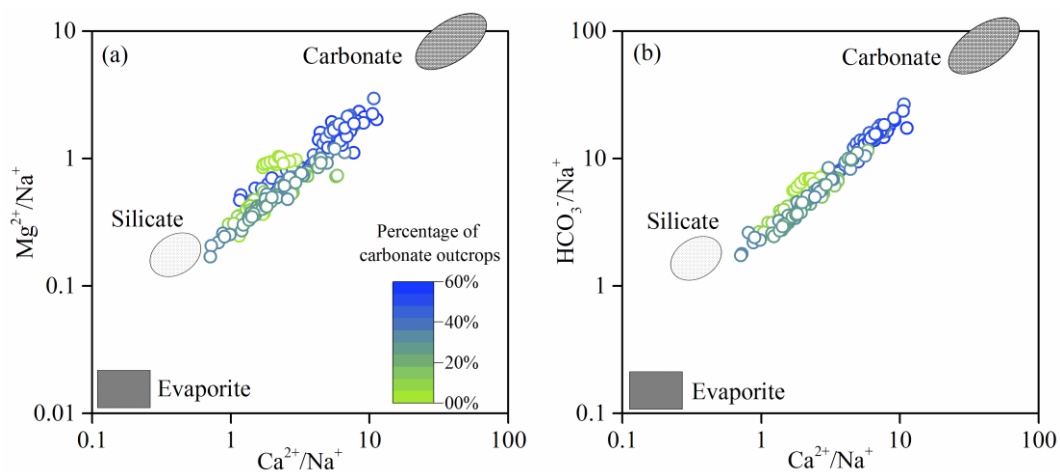
325 **5 Discussion**

326 **5.1 Chemical weathering rates and the controlling factors**

327 **5.1.1 Chemical weathering rates**

328 Atmospheric precipitation inputs, anthropogenic inputs (here refer to the acid deposition and
 329 AMD) and chemical weathering of rocks and minerals as the major sources contributed to the

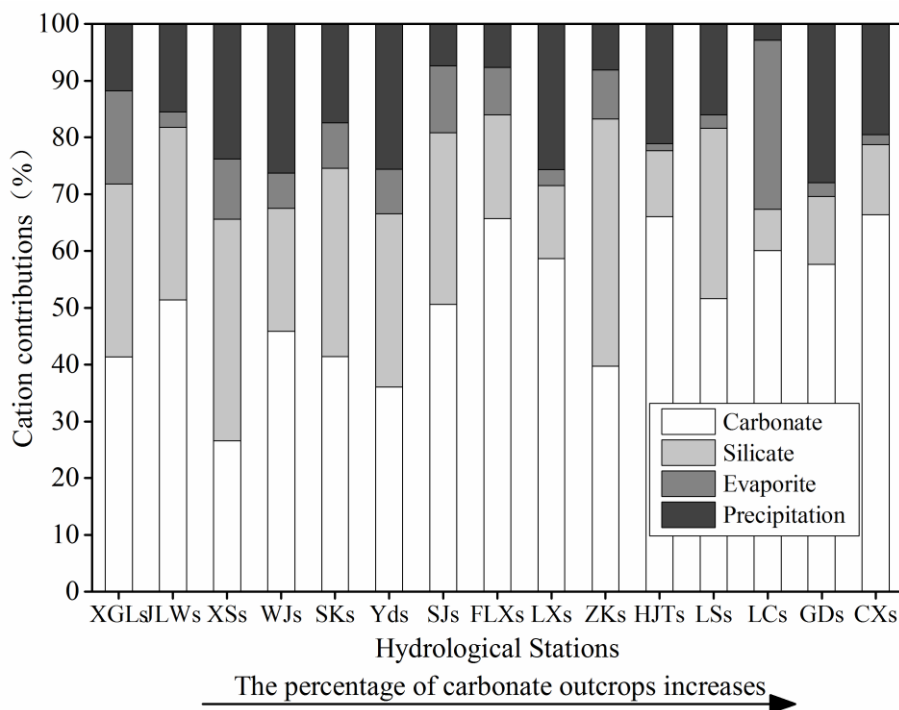
330 hydrochemistry in the river basin. Previous studies have shown that rock weathering contributions
 331 to major element composition of the river can be interpreted in terms of mixing among three main
 332 end-members: the weathering products of carbonates, silicates and evaporites (Cao et al., 2016b;
 333 Négrel et al., 1993; Ollivier et al., 2010). The river water samples in the Beijiing River Basin were
 334 displayed on the plots of Na-normalized molar ratios (Fig. 5). In these plots, the contributions
 335 from carbonate weathering correspond to the trend toward high- Ca^{2+} end-member close to the top
 336 right corner, while silicate weathering correspond to the trend toward to high- Na^+ end-member
 337 close to the low-left corner. It was clear that the samples with high ratio of carbonate outcrop had
 338 the highest molar ratios of $\text{Ca}^{2+}/\text{Na}^+$, $\text{Mg}^{2+}/\text{Na}^+$ and $\text{HCO}_3^-/\text{Na}^+$, which made the samples located
 339 toward to the carbonate weathering end-member. However, the samples with low $\text{Ca}^{2+}/\text{Na}^+$,
 340 $\text{Mg}^{2+}/\text{Na}^+$ and $\text{HCO}_3^-/\text{Na}^+$ ratios showed the influence of silicate weathering. In addition, major
 341 ion compositions of the Beijiing River were mainly contributed by the weathering of carbonates
 342 and silicates, and showed little contribution of evaporite weathering.



343
 344 **Fig. 5** Mixing diagrams using Na-normalized molar ratios: (a) $\text{Mg}^{2+}/\text{Na}^+$ vs. $\text{Ca}^{2+}/\text{Na}^+$ (b)
 345 $\text{HCO}_3^-/\text{Na}^+$ vs. $\text{Ca}^{2+}/\text{Na}^+$ for the Beijiing River Basin. The color ramp showed the percentage of
 346 carbonate outcrops

347 Based on the chemical balance method, the calculated contributions of different sources to

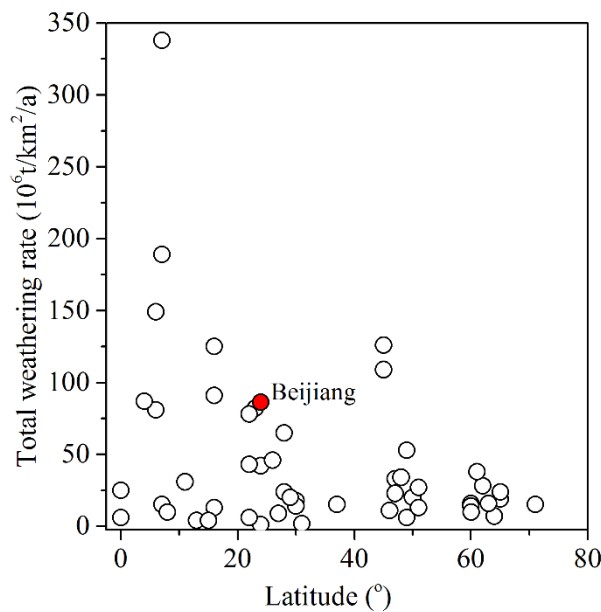
348 the total cationic loads were presented in Fig. 6. The results showed that carbonate weathering was
 349 the most important mechanism controlling the local hydrochemistry, and contributed
 350 approximately 50.06% (10.96%~79.96%) of the total cationic loads. Silicate weathering and
 351 atmospheric precipitation inputs accounted for 25.71% (5.55%~70.38%) and 17.92% (0~46.95%),
 352 respectively. Evaporite weathering had the minimum contribution with an average of 6.31%
 353 (0~24.36%) to the total cationic loads.



354 **The percentage of carbonate outcrops increases** →
 355 **Fig. 6 Calculate contributions (in %) from the different hydrological stations to the total cationic**
 356 **load in the Beijiang River Basin. The cationic loads were the sum of Na⁺, K⁺, Ca²⁺ and Mg²⁺**

357 The result of chemical weathering rates was listed in Table 2. The carbonate weathering
 358 contributes about 70% of the total chemical weathering, and the average of carbonate and silicate
 359 weathering rate in the Beijiang River Basin were 61.15 and 25.31 t·km⁻²·a⁻¹, respectively. In
 360 addition, chemical weathering rates showed significantly seasonal variations with the highest
 361 carbonate and silicate weathering rates in May (16.75 and 5.50 t·km⁻²·month⁻¹, respectively) and

362 the lowest carbonate and silicate weathering rates in February (0.95 and 0.39 t·km⁻²·month⁻¹,
 363 respectively). Gaillardet et al. (1999a) reported the chemical weathering rate of major rivers all
 364 over the world and found that the hyperactive zone with high chemical weathering rate is
 365 generally located between the latitude 0-30° and our study belongs to this area (Fig. 7). The factors
 366 influence the balance between CWR and SWR would be further discussed in the following parts.



367

368 **Fig. 7 Relationship between latitude and total weathering rate (TWR)**

369 **Table 2 The annual discharge, catchment area, carbonate and silicate outcrops proportions, and**
 370 **calculated weathering rates of carbonate and silicate of 15 subcatchments in the Beijiang River**

ID	Annual discharge (10 ⁸ m ³ /a)	Catchment area (km ²)	Percentages of carbonate (%)	Percentages of silicate (%)	Carbonate weathering rate -CWR (t km ⁻² year ⁻¹)	Silicate weathering rate -SWR (t km ⁻² year ⁻¹)	Total weathering rate -TWR (t km ⁻² year ⁻¹)
JLWs	2.23	281.13	2.95	97.05	18.63	14.94	33.56
CXs	4.06	392.35	57.44	42.56	74.21	11.42	85.64
HJTs	11.54	503.02	41.99	55.83	169.12	29.73	198.85
ZKs	16.38	1655.22	34.60	61.81	35.03	24.14	59.17
XGLs	13.56	1863.02	0.38	93.07	25.75	13.96	39.72
WJs	19.11	1960.99	12.51	73.87	55.00	17.43	72.43
LXs	56.37	2458.06	34.32	64.07	178.71	29.39	208.10
LCs	58.74	5278.14	49.67	50.21	79.70	20.59	100.29

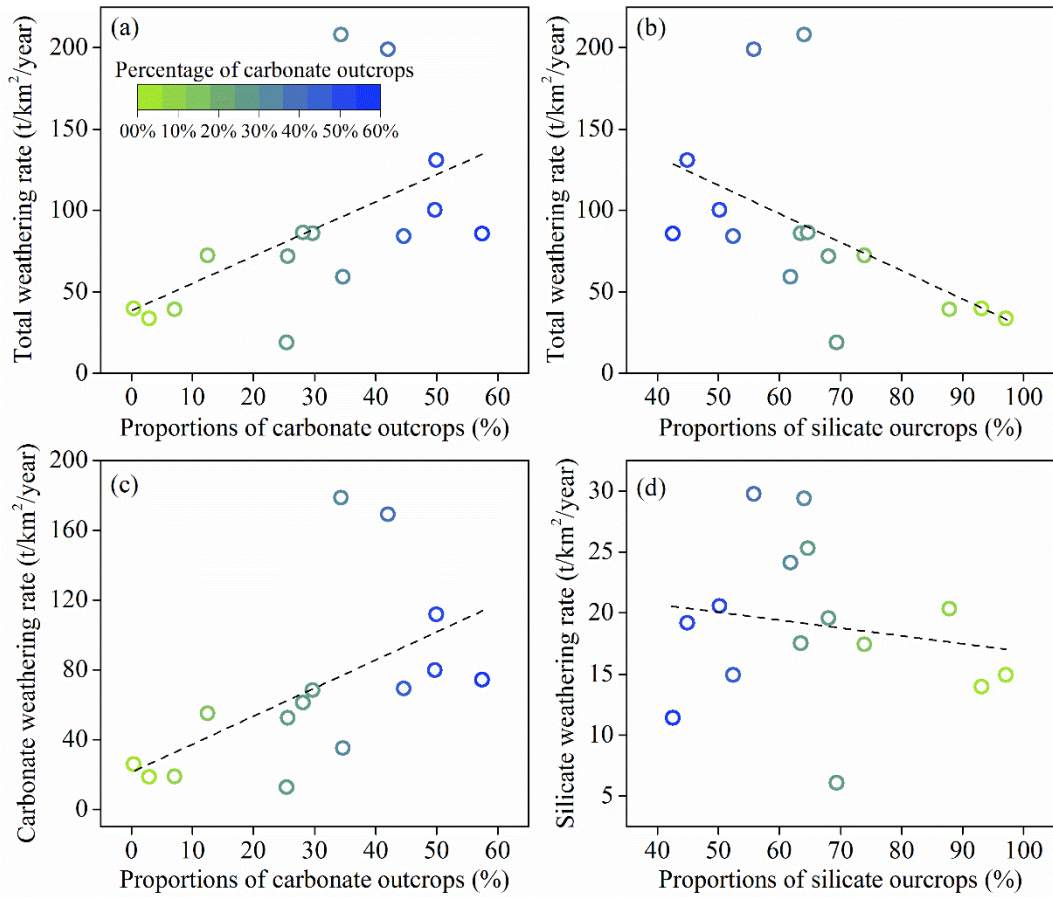
LSs	74.83	6994.69	44.59	52.44	69.28	14.94	84.22
XSs	62.11	7497.01	7.09	87.81	18.85	20.35	39.20
GDs	137.81	9028.38	49.93	44.93	111.73	19.19	130.92
SKs	49.51	17417.24	25.43	69.35	12.71	6.11	18.82
YDs	191.07	18234.64	25.63	68.05	52.37	19.59	71.95
FLXs	396.25	34232.34	29.68	63.49	68.38	17.53	85.91
SJs(Average)	450.90	38538.06	28.12	64.65	61.15	25.31	86.46

371 **5.1.2 Factors affecting chemical weathering**

372 Many factors control the chemical weathering rates, including terrain, geotectonic properties,
373 lithology, land cover, climatic conditions (temperature, precipitation, etc.), and hydrological
374 characteristics (Ding et al., 2017; Gislason et al., 2009; Hagedorn and Cartwright, 2009). For this
375 study, the lithology, hydrological characteristics and geomorphology was selected as the major
376 factors to be discussed.

377 **5.1.2.1 Lithology**

378 Among all the factors controlling the chemical weathering rates, lithology is one of the most
379 important factors because different type of rocks has different weathering abilities (Viers et al.,
380 2014). The TWR had a significant positive correlation ($p<0.01$) with the ratios of the proportion of
381 carbonate and a non-significant positive correlation with that of silicate outcrops (Fig. 8a, b).
382 Furthermore, a significant correlation ($p<0.01$) was found between the CWR and proportion of
383 carbonate outcrops (Fig. 8c), but the correlation between the SWR and the proportion of silicate
384 outcrops was low and not statistically significant ($p>0.05$, Fig. 8d). The correlation analysis
385 confirmed that carbonate outcrops ratios was the sensitive factor controlling the chemical
386 weathering rates and the rapid kinetics of carbonate dissolution played an important role in
387 weathering rates in the Beijiing River Basin.



388

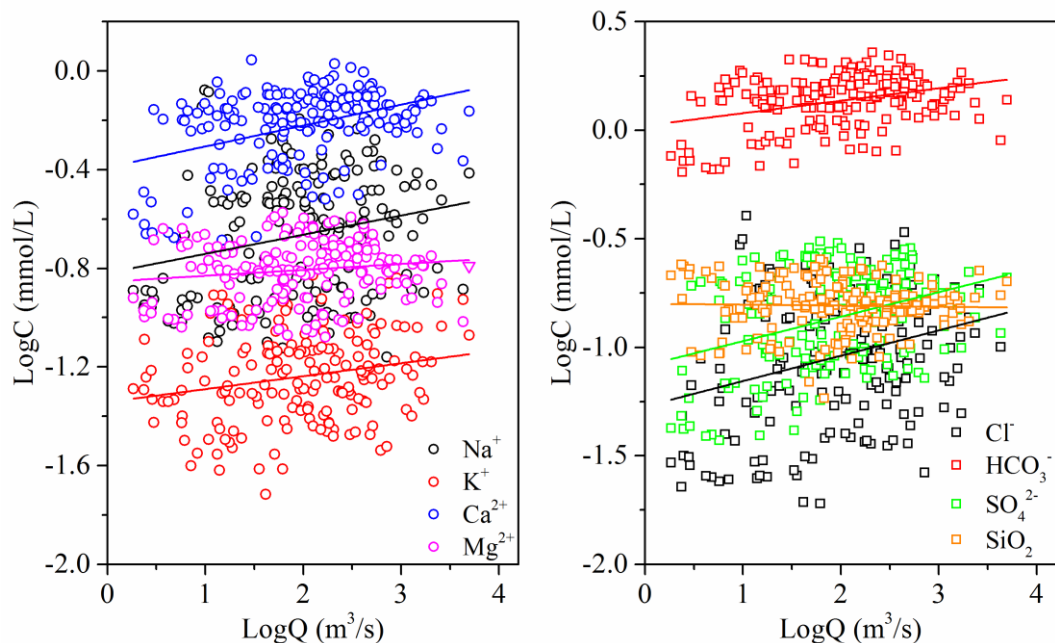
389 **Fig. 8 The relationships between weathering rates and the proportions of carbonate or silicate**
 390 **outcrops**

391 **5.1.2.2 Runoff**

392 Chemical weathering is a combination of two processes, including dissolution of primary
 393 minerals and precipitation of secondary minerals growth (Eiriksdottir et al., 2011; Hartmann et al.,
 394 2014a; Liu et al., 2013). The dissolution process is quite related to the precipitation and runoff. In
 395 general, river water chemistry is usually diluted by river runoff (Q), and this dilution effect is
 396 variable in different basins (Rao et al., 2019). The dilution effects of major element caused by
 397 increasing water flow can be expressed by log linear equation, the standard rating relationship (Li
 398 et al., 2014; Walling, 1986; Zhang et al., 2007a):

399
$$C_i = aQ^b \tag{33}$$

400 where C_i is the concentration of element i (mmol/L), Q is the water discharge (m^3/s), a is the
 401 regression constant and b is the regression exponent. The linear fitting result was showed by Fig. 9
 402 and the parameters b for major elements obtained from the dataset were 0.08 (Na^+), 0.05 (K^+),
 403 0.08 (Ca^{2+}), 0.02 (Mg^{2+}), 0.06 (HCO_3^-), 0.12 (Cl^-), 0.11 (SO_4^{2-}) and -0.005 (SiO_2), respectively. In
 404 many cases, b ranges from -1 to 0 due to the chemical variables that are influenced in various
 405 ways and various extents. However, in our study area, the values of b were positive and not
 406 comparable to the observations in the major Asian River such as the Yangtze (Chen et al., 2002a),
 407 the Yellow (Chen et al., 2005), the Pearl Rivers (Zhang et al., 2007a) and the Mekong River (Li et
 408 al., 2014). This suggested additional and significant solute sources in the river basin that might
 409 contribute and compensate considerably the effect of dilution by precipitation. The difference of
 410 slope for individual dissolved components at different stations reflected the different sources and
 411 the solubility of source materials.



412
 413 **Fig. 9 The relationship between major ion concentrations and runoff (Q) in logarithmic scales**

414 Due to the compensation effect of chemical weathering, significant positive linear

415 relationship was detected between Q and TWR, CWR and SWR. So that, the linear regression
 416 analysis between Q and TWR, CWR and SWR were conducted to further reveal the effect of
 417 runoff on chemical weathering rate. The slope of the liner regression equations for all 15
 418 hydrological station watersheds in the Beijiang River Basin were summarized in Table 3. The
 419 linear relations indicated that the increase of runoff could accelerate the chemical weathering rates,
 420 but the variations of K values revealed that the degrees of influences were different due to multiple
 421 factor influence, such as the influence of geomorphology.

422 **Table 3 The slope of the liner regression equation between runoff (Q) and total weathering rate**
 423 **(TWR), carbonate weathering rate (CWR) and silicate weathering rate (SWR)**

Hydrological stations	Total weathering rate =K ₁ Q		Carbonate weathering rate =K ₂ Q		Silicate weathering rate =K ₃ Q	
	K ₁	R ²	K ₂	R ²	K ₃	R ²
JLWs	0.3912	0.9983	0.2091	0.9962	0.1821	0.9993
CXs	0.6492	0.9335	0.5631	0.9250	0.0860	0.9378
HJTs	0.5117	0.9689	0.4421	0.9613	0.0695	0.9939
ZKs	0.0953	0.9679	0.0525	0.7612	0.0429	0.8037
XGLs	0.0835	0.9781	0.0558	0.9741	0.0278	0.9817
WJs	0.1017	0.9985	0.0842	0.9965	0.0175	0.8835
LXs	0.0968	0.9816	0.0843	0.9778	0.0125	0.9914
LCs	0.0486	0.8983	0.0401	0.8672	0.0085	0.9739
LSs	0.0359	0.9654	0.0286	0.9570	0.0073	0.9423
XSs	0.0180	0.9806	0.0080	0.9681	0.0100	0.9571
GDs	0.0252	0.9969	0.0216	0.9974	0.0036	0.9900
SKs	0.0116	0.9802	0.0083	0.9822	0.0033	0.9547
Yds	0.0106	0.9963	0.0081	0.9936	0.0026	0.9240
FLXs	0.0050	0.9681	0.0039	0.9485	0.0010	0.9949
SJs	0.0053	0.9883	0.0037	0.9706	0.0016	0.9778

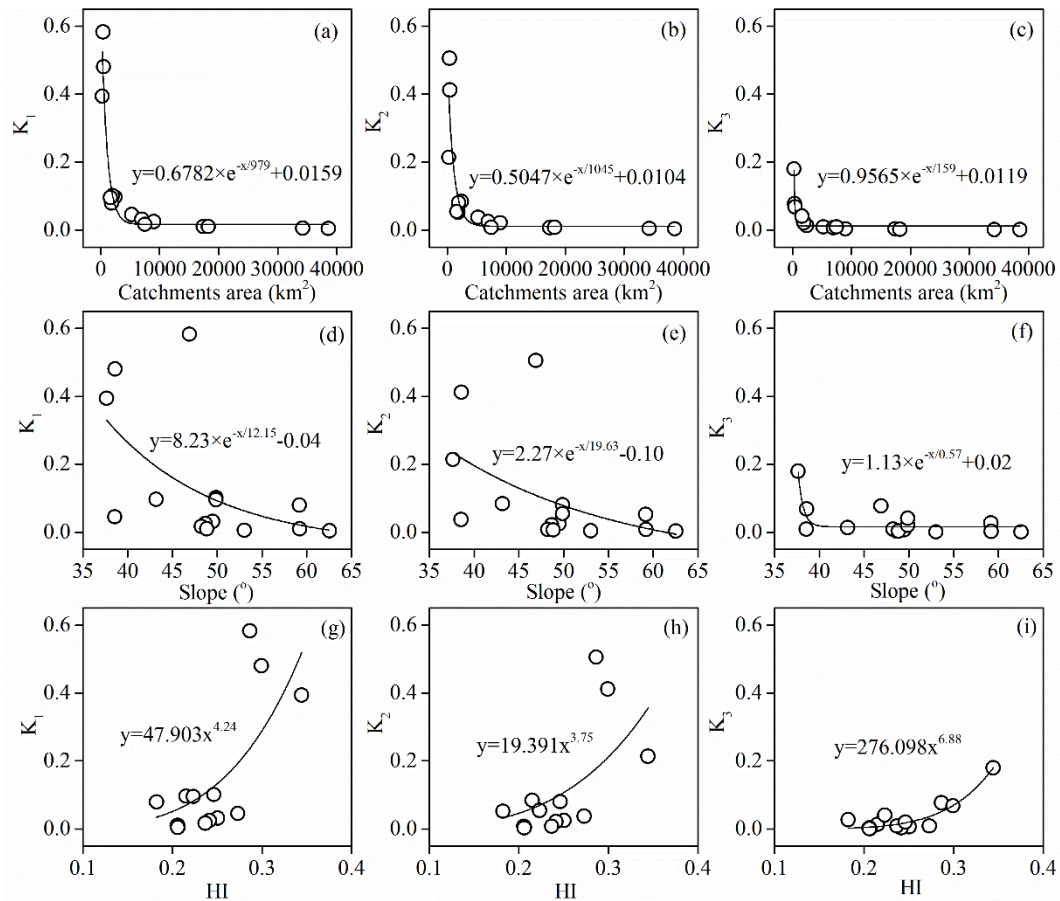
424 **5.1.2.3 Geomorphology**

425 The geomorphology factors including catchment area, average slope and HI, which could quite

426 influence the runoff generation process and physical and chemical weathering, were selected to give
427 a further explanation of the variation of K values. As showed in Fig. 10a, the K values were found a
428 non-linear relationship with the areas of subcatchment and could be fitted by exponential decay
429 model, which showed that the K values decreased dramatically with the initial increasing of area
430 and quickly become stable after reaching the threshold. The threshold value for K_1 , K_2 and K_3 was
431 about 5000 km². It indicated that the compensation effect was more significant in small catchment.

432 The average topographic slope of each subcatchment ranged from 37° to 63°. With the
433 increasing of average slope, the residence time of both surface water and groundwater decrease.
434 Kinetics of carbonate and silicate reactions was determined by the reaction time which could be
435 related by the residence time of water. In our study area, the K values showed non-linear negative
436 correlation with average slope (Fig. 10e, f, g). When the average slope increase, the resulted small
437 residence time (time of water-rock reactions) make the compensation effect also weak in the study
438 area.

439 Hypsometric analysis showed that the HI ranged from 0.18 to 0.34. According to the
440 empirical classification by HI ($HI > 0.6$, inequilibrium or young stage, $0.35 < HI \leq 0.6$,
441 equilibrium or mature stage, $HI \leq 0.35$, monadnock or old age), the geomorphological
442 development in the Beijiang River was recognized as the old age, which reflect the erodible
443 degree and erosion trend of the geomorphology was high. Furthermore, the non-linear positive
444 correlations between HI and K values (Fig. 10g, h, i) also addressed that geomorphology
445 development have significant influence on chemical weathering and relating CO₂ consumption
446 processes.



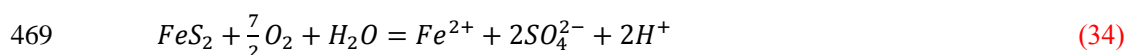
447
 448 **Fig. 10 The relationships between K values and catchments area (a, b, c), average slope (d, e, f)**
 449 **and HI (g, h, i) for the Beijiang River.**

450 **5.2 Temporary and net sink of atmospheric CO₂**

451 **5.2.1 Sulfate origin and DIC apportionment**

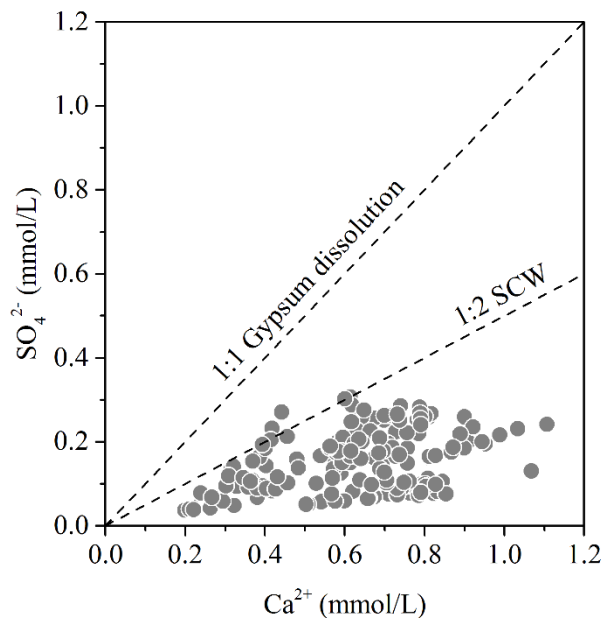
452 The successful application of DIC apportionment calculation mentioned in section 3.22 is
 453 depended on the origins of sulfate (SO₄²⁻). Three origins of SO₄²⁻ should be discriminated
 454 including atmospheric acid deposition (Larssen and Carmichael, 2000), acid mining discharge
 455 (AMD) (Li et al., 2018; Li et al., 2019) and chemical weathering of evaporite such as the
 456 dissolution of gypsum (Appelo and Postma, 2005). Acid rain events occurred frequently in South
 457 and East China after 1980 (Larssen et al., 2006). The pH isolines based on data from 86
 458 monitoring stations (Larssen et al., 2006) showed that in the Beijiang River the rain pH was lower
 459 than 4.5 and our monitoring dataset also proved this result. Sulfur wet deposition estimated based

460 on the observed bulk wet sulfur deposition data and the RAINS-Asia model (Larssen and
461 Carmichael, 2000) ranged from 2000-5000 eq ha⁻¹ a⁻¹, which showed that the acid sulfur
462 deposition was one of the most important sources of river sulfate. In addition, considering the
463 abundant ore resources in the Beijiang River, the second possible source of SO₄²⁻ is sulfide
464 oxidation due to mining. In our previous study, the SO₄²⁻ with AMD origin mainly came from the
465 tributary Wenjiang River (Wen et al., 2018). These two sources could offer sufficient chemical
466 weathering agent H₂SO₄ and actively involved in the chemical weathering due to the following
467 reaction mechanism (take carbonate for example) (Taylor et al., 1984; van Everdingen and Krouse,
468 1985).



471 The third source came from dissolution of gypsum could not offer active H₂SO₄ to induce
472 carbonate and silicate dissolution. Two evidences were summarized to indicate the absence of
473 gypsum in the study area, (1) Lithology in the river basin is composed of limestone, sandstone,
474 gneiss and glutenite. HI showed that geomorphology development has entered into the “old” age,
475 the evaporite such as halite and gypsum has been consumed by the dissolution. (2) The
476 stoichiometric relationship between Ca²⁺ and SO₄²⁻ (Fig. 11) showed that all of the samples in the
477 study area located below the 1:1 gypsum dissolution line, and they also below the 1:2 carbonate
478 weathering induced by sulfuric acid (SCW) line. These two points combined gave the evidence to
479 prove the absence of contribution of gypsum dissolution to river SO₄²⁻. So that, the DIC
480 apportionment could be calculated according to equation (18) to (21) and the result of three main
481 processes (CCW, CSW and SCW) contributing to the DIC origin in the Beijiang River water are

482 showed in Table 4. It was found that CCW was the dominant origin of DIC (35%~87%) and that
483 SCW (3%~15%) and CSW (7%~59%) were non-negligible weathering processes.



484

485 **Fig. 11 Stoichiometric relationship between Ca^{2+} and SO_4^{2-} . The “SCW” means carbonate**

486

weathering induced by sulfuric acid

487

5.2.2 Temporary and net CO_2 sink

488

According to the classical view of the global carbon cycling (Berner and Kothavala, 2001),

489

the CO_2 sink induced by chemical weathering varies for different time scales. At short-term

490

timescale, carbonic acid based carbonate and silicate weathering (CCW and CSW) and transport

491

of the HCO_3^- to oceans through rivers is an important “temporary” carbon sink (Khadka et al.,

492

2014) and can be calculated by the sum of CCR_{CCW} and CCR_{CSW} . Thus, it was significant to

493

estimate the CCR of CCW and CSW (Liu and Dreybrodt, 2015; Liu et al., 2011). However, at the

494

geological timescale ($>10^6$ years), when over the timescale typical of residence time of HCO_3^- in

495

the ocean (10^5 years), the CCW is not a mechanism that can participate in the net sink of CO_2 in

496

the atmosphere because all of the atmospheric CO_2 fixed through CCW is returned to the

497

atmosphere during carbonate precipitation in the ocean. Meanwhile, in case of CSW, followed by

498 carbonate deposition, one of the two moles of CO₂ involved is transferred from the atmosphere to
499 the lithosphere in the form of carbonate rocks, while the other one returns to the atmosphere. The
500 CSW is recognized as the net sink of atmosphere CO₂. In addition, when sulfuric acid is involved
501 as a proton donor in carbonate weathering, half of the carbon dissolved to the atmospheric during
502 carbonate precipitation. Thus, SCW leads to a net release of CO₂ in ocean-atmosphere system. So
503 that the net CO₂ sink (expressed by CCR_{Net} in this study) is controlled by the DIC apportionment
504 according to equation (31).

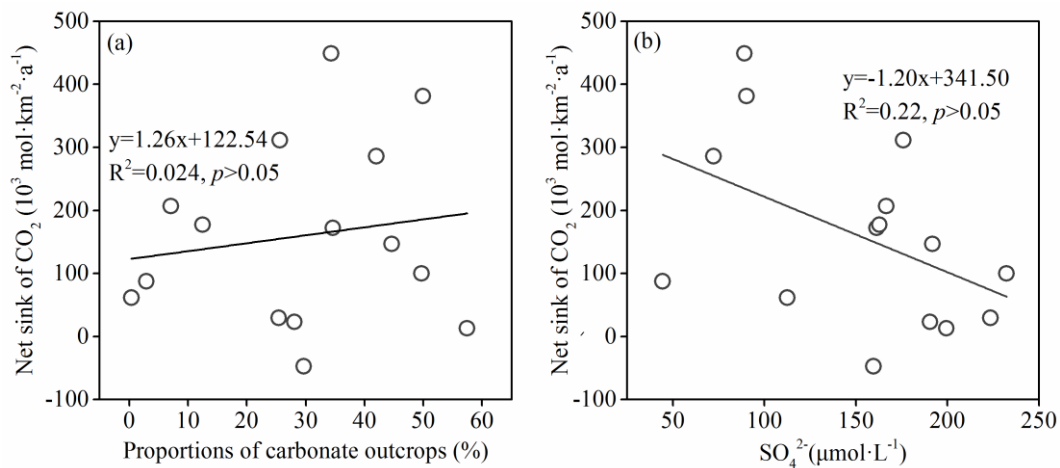
505 The results of CCR_{Total}, CCR_{CCW}, CCR_{CSW} and CCR_{Net} were summarized in Table 4. The
506 CCR_{Total} was 823.41 10³ mol km⁻² a⁻¹. Comparing with other Chinese rivers, such as the Songhua
507 River (189×10³ mol km⁻² a⁻¹) (Cao et al., 2015) and other rivers calculated by (Gaillardet et al.,
508 1999a) including the Heilong River (53×10³ mol km⁻² a⁻¹), the Changjiang River (609×10³ mol
509 km⁻² a⁻¹), the Huanghe River (360×10³ mol km⁻² a⁻¹), the Xijiang River (960×10³ mol km⁻² a⁻¹),
510 the Jinshajiang River (420×10³ mol km⁻² a⁻¹), the Langcangjiang River (980×10³ mol km⁻² a⁻¹),
511 the Nujiang River (1240×10³ mol km⁻² a⁻¹), the Yalongjiang River (870×10³ mol km⁻² a⁻¹), the
512 Daduhe River (1280×10³ mol km⁻² a⁻¹) and Minjiang River (660×10³ mol km⁻² a⁻¹), our study area
513 showed relative high CCR due to high chemical weathering rate. In addition, the CCR_{CCW} and
514 CCR_{CSW} were 536.59×10³ (65%) and 286.82×10³ (35%) mol km⁻² a⁻¹, respectively. Compared
515 with the “temporary” sink, the net sink of CO₂ for the Beijiang River was approximately
516 23.18×10³ mol km⁻² a⁻¹ of CO₂ sinking in the perspective of global carbon cycling. It was about 3%
517 of the “temporary” CO₂ sink. In addition, the CO₂ net sink of each sub basin were also different
518 and show large spatial variations due to heterogeneity of geology and human activities. The
519 geology showed weak correlation with the CO₂ net sink (Fig. 12a), while the SO₄²⁻ have negative

520 correlation with the CO₂ net sink (Fig. 12b). It proved that human activities (sulfur acid deposition
 521 and AMD) dramatically decreased the CO₂ net sink and even make chemical weathering a CO₂
 522 source to the atmosphere.

523 **Table 4 Calculated CO₂ consumption rate and net sink of 15 nested subcatchments in the**
 524 **Beijiang River Basin**

Hydrological stations	DIC apportionment (10 ⁹ mol/a)			“Temporary” Sink (CO ₂ consumption rate) (10 ³ mol km ⁻² a ⁻¹)			Net Sink (10 ³ mol km ⁻² a ⁻¹)
	CCW	SCW	CSW	CCR _{CCW}	CCR _{CSW}	CCR _{Total}	CCR _{Net}
JLWs	0.10	0.00	0.05	175.23	191.14	366.36	87.73
CXs	0.57	0.04	0.05	732.05	118.18	850.23	13.18
HJTs	1.57	0.06	0.34	1563.64	683.41	2247.05	286.14
ZKs	1.24	0.16	0.73	375.23	439.77	815.00	172.27
XGLs	0.85	0.14	0.37	227.05	195.91	422.95	61.59
WJs	1.76	0.17	0.87	449.32	443.18	892.50	177.50
LXs	7.30	0.40	2.61	1485.45	1060.45	2545.91	449.09
LCs	8.07	0.86	1.92	764.32	363.41	1127.95	99.77
LSs	10.13	0.42	2.48	724.55	354.32	1078.64	147.05
XSs	2.08	0.41	3.52	138.64	469.09	607.73	207.05
GDs	16.48	0.71	7.60	912.73	841.82	1754.55	381.36
SKs	4.00	0.72	1.74	114.77	100.23	215.00	29.55
YDs	14.11	1.75	13.10	386.82	718.64	1105.45	311.14
FLXs	40.38	7.74	4.46	589.77	130.45	720.23	-47.73
SJs	41.36	9.27	11.05	536.59	286.82	823.41	23.18

525



526

527 **Fig. 12 Correlations between CO₂ net sinks and proportions of proportions of carbonate (a) and**

528 **correlations between CO₂ net sinks and SO₄²⁻ (b)**

529 6 Conclusions

530 This study revealed the temporary and net sinks of atmospheric CO₂ due to chemical
 531 weathering in a subtropical hyperactive catchment with mixing carbonate and silicate lithology
 532 under the stress of chemical weathering induced by anthropogenic sulfuric acid agent. During the
 533 sampling period, the pH values ranged from 7.5 to 8.5 and TDS varied from 73.8 to 230.2 mg·L⁻¹.
 534 Ca²⁺ and HCO₃⁻ were the dominated cation and anion. Water chemical patterns and PCA showed
 535 that carbonate and silicate weathering were the most important processes controlling the local
 536 hydrochemistry. In average, carbonate and silicate weathering contributed approximately 50.06%
 537 and 25.71% of the total cationic loads, respectively.

538 The average of carbonate and silicate weathering rate in the Beijiing River Basin were 61.15
 539 and 25.31 t·km⁻²·a⁻¹, respectively. The high rate was comparable to other rivers located in the
 540 hyperactive zone between the latitude 0-30°. **The lithology, runoff and geomorphology had**
 541 **significant influences on the chemical weathering rate.** (1) Due to the difference between kinetics
 542 of carbonate and silicate dissolution processes, the proportion of carbonate outcrops had
 543 significant positive correlation with the chemical weathering rate and confirmed that carbonate

544 outcrops ratios was the sensitive factor controlling the chemical weathering rates and the rapid
545 kinetics of carbonate dissolution played an important role in weathering rates. (2) **Runoff mainly**
546 **controlled the season variations and the dilution effect was weak in the study area.** Due to the
547 compensation effect of chemical weathering, significant positive linear relationship was detected
548 between Q and TWR, CWR and SWR. (3) The geomorphology factors such as slope and HI had
549 non-linear correlation on chemical weathering rate and showed significant scale effect, which
550 revealed the complexity in chemical weathering processes.

551 DIC apportionment showed that CCW was the dominant origin of DIC (35%-87%) and that
552 SCW (3%-15%) and CSW (7%-59%) were non-negligible weathering processes. The CCR_{Total} was
553 $823.41 \times 10^3 \text{ mol km}^{-2} \text{ a}^{-1}$, relative high CCR due to high chemical weathering rate. In addition, the
554 CCR_{CCW} and CCR_{CSW} were 536.59×10^3 (65%) and 286.82×10^3 (35%) $\text{mol km}^{-2} \text{ a}^{-1}$, respectively.
555 Compared with the “temporary” sink, the net sink of CO_2 for the Beijiang River was
556 approximately $23.18 \times 10^3 \text{ mol km}^{-2} \text{ a}^{-1}$ of CO_2 sinking in the perspective of global carbon cycling.
557 It was about 2.82% of the “temporary” CO_2 sink. **Human activities such as sulfur acid deposition**
558 **and AMD have significantly altered the CO_2 sinks.**

559 **7 Acknowledgments**

560 This research work was financially supported by the General Program of the National Natural
561 Science Foundation of China (No.41877470), the Natural Science Foundation of Guangdong
562 Province, China (No. 2017A030313231) and the Natural Science Foundation of Guangdong
563 Province, China (No. 2017A030313229).

564 **8 Code/Data availability:** Yes.

565 **9 Author contribution:** Cao Yingjie and Tang Changyuan designed the study, carried out the
566 field work, analyzed the results, and drafted the manuscript. Xuan Yingxue and Guan Shuai
567 participated in the field sampling and laboratory analysis. Peng Yisheng reviewed and edited the
568 original draft of the manuscript. All authors read and approved the final manuscript.

569 **10 Competing interests:** No.

570 **References**

- 571 Appelo, C. A. J., and Postma, D.: *Geochemistry, groundwater and pollution*, CRC press, 2005.
- 572 Berner, R. A., and Kothavala, Z.: GEOCARB III: a revised model of atmospheric CO₂ over
573 Phanerozoic time, *American Journal of Science*, 301, 182-204, 0002-9599, 2001.
- 574 Cao, Y., Tang, C., Song, X., and Liu, C.: Major ion chemistry, chemical weathering and CO₂
575 consumption in the Songhua River basin, Northeast China, *Environmental Earth Sciences*, 73,
576 7505-7516, 10.1007/s12665-014-3921-2, 2015.
- 577 Cao, Y., Tang, C., Cao, G., and Wang, X.: Hydrochemical zoning: natural and anthropogenic origins
578 of the major elements in the surface water of Taizi River Basin, Northeast China,
579 *Environmental Earth Sciences*, 75, 811, 10.1007/s12665-016-5469-9, 2016a.
- 580 Cao, Y., Tang, C., Cao, G., and Wang, X.: Hydrochemical zoning: natural and anthropogenic origins
581 of the major elements in the surface water of Taizi River Basin, Northeast China,
582 *Environmental Earth Sciences*, 75, 1-14, 2016b.
- 583 Chen, J., Wang, F., Xia, X., and Zhang, L.: Major element chemistry of the Changjiang (Yangtze
584 River), *Chemical Geology*, 187, 231-255, 2002a.
- 585 Chen, J., Wang, F., Xia, X., and Zhang, L.: Major element chemistry of the Changjiang (Yangtze
586 River), *Chemical Geology*, 187, 231-255, 2002b.
- 587 Chen, J., Wang, F., Meybeck, M., He, D., Xia, X., and Zhang, L.: Spatial and temporal analysis of
588 water chemistry records (1958–2000) in the Huanghe (Yellow River) basin, *Global
589 biogeochemical cycles*, 19, 2005.
- 590 Ding, H., Liu, C.-Q., Zhao, Z.-Q., Li, S.-L., Lang, Y.-C., Li, X.-D., Hu, J., and Liu, B.-J.:
591 Geochemistry of the dissolved loads of the Liao River basin in northeast China under
592 anthropogenic pressure: Chemical weathering and controlling factors, *Journal of Asian Earth
593 Sciences*, 138, 657-671, <https://doi.org/10.1016/j.jseaes.2016.07.026>, 2017.
- 594 Donnini, M., Frondini, F., Probst, J.-L., Probst, A., Cardellini, C., Marchesini, I., and Guzzetti, F.:
595 Chemical weathering and consumption of atmospheric carbon dioxide in the Alpine region,
596 *Global and Planetary Change*, 136, 65-81, <https://doi.org/10.1016/j.gloplacha.2015.10.017>,
597 2016.
- 598 Dosseto, A., Bourdon, B., Gaillardet, J., Allègre, C. J., and Filizola, N.: Time scale and conditions of
599 weathering under tropical climate: Study of the Amazon basin with U-series, *Geochimica et
600 Cosmochimica Acta*, 70, 71-89, <https://doi.org/10.1016/j.gca.2005.06.033>, 2006.
- 601 Edmond, J. M., Palmer, M. R., Measures, C. I., Brown, E. T., and Huh, Y.: Fluvial geochemistry of
602 the eastern slope of the northeastern Andes and its foredeep in the drainage of the Orinoco in

603 Colombia and Venezuela, *Geochimica et Cosmochimica Acta*, 60, 2949-2974,
604 [https://doi.org/10.1016/0016-7037\(96\)00142-1](https://doi.org/10.1016/0016-7037(96)00142-1), 1996.

605 Eiriksdottir, E. S., Gislason, S. R., and Oelkers, E. H.: Does runoff or temperature control chemical
606 weathering rates?, *Applied Geochemistry*, 26, S346-S349,
607 <https://doi.org/10.1016/j.apgeochem.2011.03.056>, 2011.

608 Fernandes, A. M., Conceição, F. T. d., Spatti Junior, E. P., Sardinha, D. d. S., and Mortatti, J.:
609 Chemical weathering rates and atmospheric/soil CO₂ consumption of igneous and
610 metamorphic rocks under tropical climate in southeastern Brazil, *Chemical Geology*, 443,
611 54-66, <https://doi.org/10.1016/j.chemgeo.2016.09.008>, 2016.

612 Gaillardet, J., Dupré, B., Louvat, P., and Allègre, C. J.: Global silicate weathering and CO₂
613 consumption rates deduced from the chemistry of large rivers, *Chemical Geology*, 159, 3-30,
614 [https://doi.org/10.1016/S0009-2541\(99\)00031-5](https://doi.org/10.1016/S0009-2541(99)00031-5), 1999a.

615 Gaillardet, J., Dupré, B., Louvat, P., and Allègre, C. J.: Global silicate weathering and CO₂
616 consumption rates deduced from the chemistry of large rivers, *Chemical Geology*, 159, 3-30,
617 [https://doi.org/10.1016/S0009-2541\(99\)00031-5](https://doi.org/10.1016/S0009-2541(99)00031-5), 1999b.

618 Galy, A., and France-Lanord, C.: Weathering processes in the Ganges–Brahmaputra basin and the
619 riverine alkalinity budget, *Chemical Geology*, 159, 31-60,
620 [https://doi.org/10.1016/S0009-2541\(99\)00033-9](https://doi.org/10.1016/S0009-2541(99)00033-9), 1999.

621 Gao, Q., Tao, Z., Huang, X., Nan, L., Yu, K., and Wang, Z.: Chemical weathering and CO₂
622 consumption in the Xijiang River basin, South China, *Geomorphology*, 106, 324-332,
623 <https://doi.org/10.1016/j.geomorph.2008.11.010>, 2009.

624 Garrels, R. M.: The carbonate-silicate geochemical cycle and its effect on atmospheric carbon
625 dioxide over the past 100 million years, *Am J Sci*, 283, 641-683, 1983.

626 Gibbs, R. J.: Water chemistry of the Amazon River, *Geochimica et Cosmochimica Acta*, 36,
627 1061-1066, [https://doi.org/10.1016/0016-7037\(72\)90021-X](https://doi.org/10.1016/0016-7037(72)90021-X), 1972.

628 Gislason, S. R., Oelkers, E. H., Eiriksdottir, E. S., Kardjilov, M. I., Gisladottir, G., Sigfusson, B.,
629 Snorrason, A., Elefsen, S., Hardardottir, J., Torssander, P., and Oskarsson, N.: Direct evidence
630 of the feedback between climate and weathering, *Earth and Planetary Science Letters*, 277,
631 213-222, <https://doi.org/10.1016/j.epsl.2008.10.018>, 2009.

632 Guo, J., Wang, F., Vogt, R. D., Zhang, Y., and Liu, C. Q.: Anthropogenically enhanced chemical
633 weathering and carbon evasion in the Yangtze Basin, *Scientific Reports*, 5, 11941, 2015.

634 Hagedorn, B., and Cartwright, I.: Climatic and lithologic controls on the temporal and spatial
635 variability of CO₂ consumption via chemical weathering: An example from the Australian
636 Victorian Alps, *Chemical Geology*, 260, 234-253,
637 <https://doi.org/10.1016/j.chemgeo.2008.12.019>, 2009.

638 Hartmann, J., Jansen, N., Dürr, H. H., Kempe, S., and Köhler, P.: Global CO₂-consumption by
639 chemical weathering: What is the contribution of highly active weathering regions?, *Global
640 and Planetary Change*, 69, 185-194, <https://doi.org/10.1016/j.gloplacha.2009.07.007>, 2009.

641 Hartmann, J., Moosdorf, N., Lauerwald, R., Hinderer, M., and West, A. J.: Global chemical
642 weathering and associated P-release - The role of lithology, temperature and soil properties,
643 *Chemical Geology*, 363, 145-163, <https://doi.org/10.1016/j.chemgeo.2013.10.025>, 2014a.

644 Hartmann, J., West, J., Renforth, P., Köhler, P., Rocha, C. D. L., Wolf-Gladrow, D., Dürr, H., and
645 Scheffran, J.: Enhanced chemical weathering as a sink for carbon dioxide, a nutrient source and
646 a strategy to mitigate ocean acidification, *Reviews of Geophysics*, 2014b.

647 He Jiangyi, Z. D., Zhao zhiqi: Spatial and temporal variations in hydrochemical composition of
648 river water in Yellow River Basin, China, *Chinese Journal of Ecology*, 1-12, 2017.

649 Hercod, D. J., Brady, P. V., and Gregory, R. T.: Catchment-scale coupling between pyrite oxidation
650 and calcite weathering, *Chemical Geology*, 151, 259-276,
651 [https://doi.org/10.1016/S0009-2541\(98\)00084-9](https://doi.org/10.1016/S0009-2541(98)00084-9), 1998.

652 Huh, Y., and Edmond, J. M.: The fluvial geochemistry of the rivers of Eastern Siberia: III.
653 Tributaries of the Lena and Anabar draining the basement terrain of the Siberian Craton and the
654 Trans-Baikal Highlands, *Geochimica et Cosmochimica Acta*, 63, 967-987,
655 [https://doi.org/10.1016/S0016-7037\(99\)00045-9](https://doi.org/10.1016/S0016-7037(99)00045-9), 1999.

656 Jiang, H., Liu, W., Xu, Z., Zhou, X., Zheng, Z., Zhao, T., Zhou, L., Zhang, X., Xu, Y., and Liu, T.:
657 Chemical weathering of small catchments on the Southeastern Tibetan Plateau I: Water sources,
658 solute sources and weathering rates, *Chemical Geology*, 500, 159-174,
659 <https://doi.org/10.1016/j.chemgeo.2018.09.030>, 2018.

660 Kempe, S., and Degens, E. T.: An early soda ocean?, *Chemical Geology*, 53, 95-108,
661 [https://doi.org/10.1016/0009-2541\(85\)90023-3](https://doi.org/10.1016/0009-2541(85)90023-3), 1985.

662 Khadka, M. B., Martin, J. B., and Jin, J.: Transport of dissolved carbon and CO₂ degassing from a
663 river system in a mixed silicate and carbonate catchment, *Journal of Hydrology*, 513, 391-402,
664 <https://doi.org/10.1016/j.jhydrol.2014.03.070>, 2014.

665 Larssen, T., and Carmichael, G. R.: Acid rain and acidification in China: the importance of base
666 cation deposition, *Environmental Pollution*, 110, 89-102,
667 [https://doi.org/10.1016/S0269-7491\(99\)00279-1](https://doi.org/10.1016/S0269-7491(99)00279-1), 2000.

668 Larssen, T., Lydersen, E., Tang, D., He, Y., Gao, J., Liu, H., Duan, L., Seip, H. M., Vogt, R. D.,
669 Mulder, J., Shao, M., Wang, Y., Shang, H., Zhang, X., Solberg, S., Aas, W., Okland, T.,
670 Eilertsen, O., Angell, V., Li, Q., Zhao, D., Xiang, R., Xiao, J., and Luo, J.: Acid Rain in China,
671 *Environmental Science & Technology*, 40, 418-425, 10.1021/es0626133, 2006.

672 Lenton, T. M., and Britton, C.: Enhanced carbonate and silicate weathering accelerates recovery
673 from fossil fuel CO₂ perturbations, *Global Biogeochemical Cycles*, 20,
674 10.1029/2005gb002678, 2006.

675 Li, R., Tang, C., Cao, Y., Jiang, T., and Chen, J.: The distribution and partitioning of trace metals (Pb,
676 Cd, Cu, and Zn) and metalloid (As) in the Beijiang River, *Environmental Monitoring and
677 Assessment*, 190, 399, 10.1007/s10661-018-6789-x, 2018.

678 Li, R., Tang, C., Li, X., Jiang, T., Shi, Y., and Cao, Y.: Reconstructing the historical pollution levels
679 and ecological risks over the past sixty years in sediments of the Beijiang River, South China,
680 *Science of The Total Environment*, 649, 448-460,
681 <https://doi.org/10.1016/j.scitotenv.2018.08.283>, 2019.

682 Li, S.-L., Calmels, D., Han, G., Gaillardet, J., and Liu, C.-Q.: Sulfuric acid as an agent of carbonate
683 weathering constrained by $\delta^{13}\text{C}_{\text{DIC}}$: Examples from Southwest China, *Earth and Planetary
684 Science Letters*, 270, 189-199, <https://doi.org/10.1016/j.epsl.2008.02.039>, 2008.

685 Li, S., Lu, X. X., He, M., Zhou, Y., Bei, R., Li, L., and Ziegler, A. D.: Major element chemistry in
686 the upper Yangtze River: A case study of the Longchuanjiang River, *Geomorphology*, 129,
687 29-42, <https://doi.org/10.1016/j.geomorph.2011.01.010>, 2011.

688 Li, S., Lu, X. X., and Bush, R. T.: Chemical weathering and CO₂ consumption in the Lower Mekong
689 River, *Science of The Total Environment*, 472, 162-177,
690 <https://doi.org/10.1016/j.scitotenv.2013.11.027>, 2014.

691 Liu, B., Liu, C.-Q., Zhang, G., Zhao, Z.-Q., Li, S.-L., Hu, J., Ding, H., Lang, Y.-C., and Li, X.-D.:
692 Chemical weathering under mid- to cool temperate and monsoon-controlled climate: A study
693 on water geochemistry of the Songhuajiang River system, northeast China, *Applied*
694 *Geochemistry*, 31, 265-278, <https://doi.org/10.1016/j.apgeochem.2013.01.015>, 2013.

695 Liu, Z., Dreybrodt, W., and Liu, H.: Atmospheric CO₂ sink: Silicate weathering or carbonate
696 weathering?, *Applied Geochemistry*, 26, S292-S294,
697 <https://doi.org/10.1016/j.apgeochem.2011.03.085>, 2011.

698 Liu, Z., and Dreybrodt, W.: Significance of the carbon sink produced by H₂O-carbonate-CO₂-
699 aquatic phototroph interaction on land, *Science Bulletin*, 60, 182-191, 2095-9273, 2015.

700 Ludwig, W., Amiotte-Suchet, P., Munhoven, G., and Probst, J.-L.: Atmospheric CO₂ consumption
701 by continental erosion: present-day controls and implications for the last glacial maximum,
702 *Global and Planetary Change*, 16-17, 107-120,
703 [https://doi.org/10.1016/S0921-8181\(98\)00016-2](https://doi.org/10.1016/S0921-8181(98)00016-2), 1998.

704 Meybeck, M., Dürr, H. H., and Vörösmarty, C. J.: Global coastal segmentation and its river
705 catchment contributors: A new look at land-ocean linkage, *Global Biogeochemical Cycles*, 20,
706 10.1029/2005gb002540, 2006.

707 Mora, A., Baquero, J. C., Alfonso, J. A., Pisapia, D., and Balza, L.: The Apure River: geochemistry
708 of major and selected trace elements in an Orinoco River tributary coming from the Andes,
709 Venezuela, *Hydrological Processes*, 24, 3798-3810, 10.1002/hyp.7801, 2010.

710 Mortatti, J., and Probst, J.-L.: Silicate rock weathering and atmospheric/soil CO₂ uptake in the
711 Amazon basin estimated from river water geochemistry: seasonal and spatial variations,
712 *Chemical Geology*, 197, 177-196, [https://doi.org/10.1016/S0009-2541\(02\)00349-2](https://doi.org/10.1016/S0009-2541(02)00349-2), 2003.

713 Négrel, P., Allègre, C. J., Dupré, B., and Lewin, E.: Erosion sources determined by inversion of
714 major and trace element ratios and strontium isotopic ratios in river water: The Congo Basin
715 case, *Earth and Planetary Science Letters*, 120, 59-76,
716 [https://doi.org/10.1016/0012-821X\(93\)90023-3](https://doi.org/10.1016/0012-821X(93)90023-3), 1993.

717 Ollivier, P., Hamelin, B., and Radakovitch, O.: Seasonal variations of physical and chemical erosion:
718 A three-year survey of the Rhone River (France), *Geochimica et Cosmochimica Acta*, 74,
719 907-927, <https://doi.org/10.1016/j.gca.2009.10.037>, 2010.

720 PIKE, R. J., and WILSON, S. E.: Elevation-Relief Ratio, Hypsometric Integral, and Geomorphic
721 Area-Altitude Analysis, *GSA Bulletin*, 82, 1079-1084,
722 10.1130/0016-7606(1971)82[1079:erhiag]2.0.co;2, 1971.

723 Ran, X., Yu, Z., Yao, Q., Chen, H., and Mi, T.: Major ion geochemistry and nutrient behaviour in the
724 mixing zone of the Changjiang (Yangtze) River and its tributaries in the Three Gorges
725 Reservoir, *Hydrological processes*, 24, 2481-2495, 2010.

726 Rao, W., Zheng, F., Tan, H., Yong, B., Jin, K., Wang, S., Zhang, W., Chen, T., and Wang, Y.: Major
727 ion chemistry of a representative river in South-central China: Runoff effects and controlling
728 mechanisms, *Journal of Hazardous Materials*, 378, 120755,
729 <https://doi.org/10.1016/j.jhazmat.2019.120755>, 2019.

730 Ryu, J.-S., Lee, K.-S., Chang, H.-W., and Shin, H. S.: Chemical weathering of carbonates and
731 silicates in the Han River basin, South Korea, *Chemical Geology*, 247, 66-80,
732 <https://doi.org/10.1016/j.chemgeo.2007.09.011>, 2008.

733 Singh, O., Sarangi, A., and Sharma, M. C.: Hypsometric Integral Estimation Methods and its
734 Relevance on Erosion Status of North-Western Lesser Himalayan Watersheds, *Water*

735 Resources Management, 22, 1545-1560, 10.1007/s11269-008-9242-z, 2008.

736 Spence, J., and Telmer, K.: The role of sulfur in chemical weathering and atmospheric CO₂ fluxes:
737 Evidence from major ions, δ¹³C_{DIC}, and δ³⁴S_{SO₄} in rivers of the Canadian Cordillera,
738 *Geochimica et Cosmochimica Acta*, 69, 5441-5458, <https://doi.org/10.1016/j.gca.2005.07.011>,
739 2005.

740 Stallard, R. F., and Edmond, J. M.: Geochemistry of the Amazon: 1. Precipitation chemistry and the
741 marine contribution to the dissolved load at the time of peak discharge, *Journal of Geophysical*
742 *Research: Oceans*, 86, 9844-9858, 10.1029/JC086iC10p09844, 1981.

743 Stallard, R. F., and Edmond, J. M.: Geochemistry of the Amazon: 2. The influence of geology and
744 weathering environment on the dissolved load, *Journal of Geophysical Research: Oceans*, 88,
745 9671-9688, 10.1029/JC088iC14p09671, 1983.

746 Stallard, R. F., and Edmond, J. M.: Geochemistry of the Amazon: 3. Weathering chemistry and
747 limits to dissolved inputs, *Journal of Geophysical Research: Oceans*, 92, 8293-8302,
748 10.1029/JC092iC08p08293, 1987.

749 STRAHLER, A. N.: HYPSONOMETRIC (AREA-ALTITUDE) ANALYSIS OF EROSIONAL
750 TOPOGRAPHY, *GSA Bulletin*, 63, 1117-1142,
751 10.1130/0016-7606(1952)63[1117:haoet]2.0.co;2, 1952.

752 Sun, X., Mörth, C.-M., Humborg, C., and Gustafsson, B.: Temporal and spatial variations of rock
753 weathering and CO₂ consumption in the Baltic Sea catchment, *Chemical Geology*, 466, 57-69,
754 <https://doi.org/10.1016/j.chemgeo.2017.04.028>, 2017.

755 Taylor, B. E., Wheeler, M. C., and Nordstrom, D. K.: Stable isotope geochemistry of acid mine
756 drainage: Experimental oxidation of pyrite, *Geochimica et Cosmochimica Acta*, 48,
757 2669-2678, [https://doi.org/10.1016/0016-7037\(84\)90315-6](https://doi.org/10.1016/0016-7037(84)90315-6), 1984.

758 van Everdingen, R. O., and Krouse, H. R.: Isotope composition of sulphates generated by bacterial
759 and abiological oxidation, *Nature*, 315, 395-396, 10.1038/315395a0, 1985.

760 Viers, J., Oliva, P., Dandurand, J. L., Dupré, B., and Gaillardet, J.: Chemical weathering rates, CO₂
761 consumption, and control parameters deduced from the chemical composition of rivers, 2014.

762 Walling, D. E.: Solute in river systems, *Solute Processes*, 251-327, 1986.

763 Wen, J., Tang, C., Cao, Y., Li, X., and Chen, Q.: Hydrochemical evolution of groundwater in a
764 riparian zone affected by acid mine drainage (AMD), South China: the role of river–
765 groundwater interactions and groundwater residence time, *Environmental Earth Sciences*, 77,
766 794, 10.1007/s12665-018-7977-2, 2018.

767 Wu, W., Xu, S., Yang, J., and Yin, H.: Silicate weathering and CO₂ consumption deduced from the
768 seven Chinese rivers originating in the Qinghai-Tibet Plateau, *Chemical Geology*, 249,
769 307-320, 2008.

770 Xie chenji, G. Q., Tao zhen, Liu Longhai, Lishanchi: Chemical weathering and CO₂ consumption in
771 the Dongjiang River Basin, *Acta Scientiae Circumstantiae*, 33, 2123-2133, 2013.

772 Xiong, L., Tang, G., Yuan, B., Lu, Z., Li, F., and Zhang, L.: Geomorphological inheritance for loess
773 landform evolution in a severe soil erosion region of Loess Plateau of China based on digital
774 elevation models, *Science China Earth Sciences*, 57, 1944-1952, 10.1007/s11430-014-4833-4,
775 2014.

776 Xu, Z., and Liu, C.-Q.: Water geochemistry of the Xijiang basin rivers, South China: Chemical
777 weathering and CO₂ consumption, *Applied Geochemistry*, 25, 1603-1614, 2010.

778 Zeng, C., Liu, Z., Zhao, M., and Yang, R.: Hydrologically-driven variations in the karst-related

779 carbon sink fluxes: Insights from high-resolution monitoring of three karst catchments in
 780 Southwest China, Journal of Hydrology, 533, 74-90,
 781 <https://doi.org/10.1016/j.jhydrol.2015.11.049>, 2016.

782 Zhang, J., Huang, W., Letolle, R., and Jusserand, C.: Major element chemistry of the Huanghe
 783 (Yellow River), China-weathering processes and chemical fluxes, Journal of Hydrology, 168,
 784 173-203, 1995.

785 Zhang, L., Song, X., Xia, J., Yuan, R., Zhang, Y., Liu, X., and Han, D.: Major element chemistry of
 786 the Huai River basin, China, Applied Geochemistry, 26, 293-300, 2011.

787 Zhang, S. R., Lu, X. X., Higgitt, D. L., Chen, C. T. A., Sun, H. G., and Han, J. T.: Water chemistry of
 788 the Zhujiang (Pearl River): natural processes and anthropogenic influences. Journal of
 789 Geophysical Research, 112(F1), F01011, Journal of Geophysical Research Atmospheres, 112,
 790 137-161, 2007a.

791 Zhang, S. R., Lu, X. X., Higgitt, D. L., Chen, C. T. A., Sun, H. G., and Han, J. T.: Water
 792 chemistry of the Zhujiang (Pearl River): Natural processes and anthropogenic influences, Journal of
 793 Geophysical Research: Earth Surface (2003–2012), 112, 10.1029/2006JF000493, 2007b.

794 **Supplementary material**

795 **Table S1 The major ions concentrations of rain water samples at 5 hydrological stations in the**
 796 **Beijiang River (mean±SD).**

Hydrological stations	Na ⁺ (μmol/L)	K ⁺ (μmol/L)	Ca ²⁺ (μmol/L)	Mg ²⁺ (μmol/L)	Cl ⁻ (μmol/L)	SO ₄ ²⁻ (μmol/L)	NO ₃ ⁻ (μmol/L)
XGLs	12.8±9.7	21.0±16.8	22.2±20.5	10.9±10.3	25.9±22.6	320.2±370.7	83.3±85.2
XSs	20.4±11.8	7.8±4.5	86.9±30.4	10.1±5.2	10.0±0.0	606.5±511.5	36.3±23.4
Yds	16.3±9.5	10.1±10.8	161.1±56.5	9.0±7.8	23.9±12.4	136.9±169.5	143.1±135.5
FLXs	18.8±12.3	3.2±2.5	31.1±17.7	4.2±2.7	23.1±16.6	45.4±27.5	77.1±70.4
SJs	12.6±9.2	12.5±16.3	22.9±13.8	15.4±18.1	25.4±16.0	79.0±79.8	156.7±206.4

797